

Microstructural Changes in Coal During Low-temperature Ashing*

R. W. Carling, R. M. Allen

Sandia National Laboratories
Livermore, CA 94550

and

J. B. VanderSande

Massachusetts Institute of Technology
Cambridge, MA 02139

Introduction

In the present work, the microstructural changes occurring in two U. S. coals during low temperature ashing (LTA) have been examined using a scanning transmission electron microscope (STEM) and automated image analysis in an electron microprobe. The latter, a computer based technique, can be used to provide a quantitative analysis, by species, of the mineral particles $>0.2 \mu\text{m}$ in diameter in petrographic samples of powdered coal. A full description of the operation of automated image analysis routines for coal science application may be found elsewhere(1-5). The STEM, by comparison, with its high spatial resolution for imaging and compositional analysis, can be used to examine ultra-fine mineral particles (diameters $<0.2 \mu\text{m}$) in coal(6-9), and also to directly determine the principal inorganic elements chemically bound in the organic coal matrix(9). These two techniques therefore can be used together in a complementary manner to provide a detailed characterization of the mineral matter in coal samples(9). For the present task, their ability to work directly on either raw coal or ash samples was also a great advantage.

In support of the electron optical analysis of LTA transformations, complex thermochemical calculations have also been made. These calculations serve two purposes. The first is to provide a more fundamental thermodynamic understanding of mineral matter behavior under LTA conditions. Secondly, the calculations assist the electron microscopist in identifying species by predicting the possible products of observed reactants. This serves as guide when it becomes necessary to distinguish various species by electron diffraction, rather than energy-dispersive X-ray spectrometry (as when dealing with the many oxides, sulfides, and sulfates of iron). The limitation on this computational technique is that chemical equilibrium is assumed but may not be reached over the duration of a typical LTA experiment.

*This work supported by U.S. Department of Energy, DOE, under contract DE-AC04-76DP00789.

Experimental

The coals used in the present experiments were PSOC 98, a high-volatile-C bituminous coal from Wyoming (Bed #80 seam), and PSOC 279, a high-volatile-B bituminous coal from Indiana (Indiana #3 seam) obtained from the Penn State Coal Bank. The low temperature asher used in the present work was an LTA-504 from LFE Corporation. During ashing, small specimens were removed from a sample of each coal after 1, 3, 6, 12, 24, 48, and 72 hours of ashing. These partially-ashed samples were used for subsequent STEM analyses.

Thermochemical Modeling

The complex equilibrium code used in this work was an extension of the code originally developed by Erickson(10-12) and later modified by Bessman(13). The code, SOLGASMIX-PV, has been interfaced with a data base that is a compilation of thermodynamic data from JANAF(14) and the U.S. Geological Survey(15).

The elements included in the equilibrium calculations were: H, C, O, Mg, Al, Si, S, Ca, and Fe. The numbers of moles of each element (based on the analyses of each coal) were entered as oxides. An excess of oxygen was included to simulate the oxygen-rich environment of the LTA. The equilibrium temperature was set at 150°C with a pressure of one atmosphere. The list of species investigated for equilibrium stability is too long to present here, but included all of the combinations of the above elements given in the JANAF data base as well as many carbonates, sulfates, alumino-silicates, and sodium-aluminum silicates tabulated by the U.S. Geological Survey.

Results

PSOC 98

Low temperature ashing produced radical structural changes in PSOC 98 which resulted in individual ash particles having a gauzy appearance in the STEM. Stereomicroscopic examination revealed that the "gauze" was a fine three-dimensional network with denser particles suspended within the ash matrix. STEM microanalysis showed these dense particles to be the same sort of mineral inclusions observed in the raw coal. Electron diffraction patterns taken of the ash showed crisp rings characteristic of crystalline material. Analysis of the ash matrix in the STEM revealed Ca and S, as in the raw coal matrix. With this additional compositional information, the diffraction patterns were indexed and the presence of the mineral bassanite, $\text{CaSO}_4 \cdot 1/2\text{H}_2\text{O}$, was established. The grain size of the bassanite networks forming the matrices of the ash particles was on the order of 30 nm, as determined from standard dark field images formed from portions of the bassanite ring pattern.

Subsequent X-ray diffraction analysis of the material ashed for 72 hours showed bassanite to be one of the three principal minerals found after LTA (together with quartz and kaolinite).

PSOC 279

The raw particles of PSOC 279 were similar in appearance to those of PSOC 98. The most commonly observed type of ash particle, however, consisted of an agglomeration of mineral particles, principally quartz, clays, and pyrite. These were the predominant mineral species found in the raw coal by the electron microprobe analysis. These were also the three major species found by X-ray diffraction in the material ashed for 72 hours.

"Gauzy" ash particles, very similar in appearance to those in the PSOC 98 ash, were less common than the agglomerate type but were also found in the STEM samples. The characteristic inorganic signature of the organic matrix of raw PSOC 279 particles was a combination of an Al and a Si signal. Again, the same combination was carried over into the matrices of the gauzy type or ash for this coal.

STEM examination of the low temperature ash of PSOC 279 showed that much of the pyrite in the starting coal survived the full 72 hours of ashing. This was confirmed by the X-ray diffraction analysis of the ash, as mentioned earlier. STEM analysis was also done on particles of small (<80 nm diameter) crystals. These particles were Fe and S rich, but with much lower S:Fe ratios than pyrite. A significant portion of these particles had a cubic morphology. No minerals of this type were observed during STEM examination of the raw Indiana coal.

Modeling Results

Figure 1 illustrates the stable condensed phases predicted by the equilibrium calculations for low temperature ashing conditions. The results shown are for PSOC 98 but apply as well for PSOC 279 except for the relative amounts of each specie.

Discussion

Bassanite formation is commonly observed during low temperature ashing, particularly for western coals. It is believed to form by three means: dehydration of gypsum ($\text{CaSO}_4 \cdot 2\text{H}_2\text{O}$) found in the raw coal (16,17), reaction of organic S and the mineral calcite (CaCO_3) (18), and direct reaction of organic Ca and S (19,20). These reactions have proven to be hard to distinguish, because of the difficulty of analyzing the starting mineral content of raw coal samples by conventional techniques, and the inability of these same techniques to find and examine partially-ashed

particles to observe the reaction in progress. The use of the electron-optical analysis techniques described in this paper, however, overcame both of these problems, as will now be described.

The STEM results for PSOC 98 indicate that the organic matrix of the raw coal contained Ca and S in a non-crystalline form. This is consistent with the Penn State sulfur-forms analysis which indicates that most of the S in the coal is in an organic form. It also explains the relatively small percentages of Ca-bearing minerals found by the electron microprobe, since other information indicates that PSOC 98 contains a relatively large amount of calcium.

Apparently, the organic matrix of the coal itself was the origin of the Ca and S needed for bassanite formation. The fact that calcium sulphate would form under these conditions was confirmed by the results of the thermochemical calculations (see Fig. 1) which indicated that sufficient sulfur was present in the coal to react with the calcium and prevent the formation of other species, such as calcium carbonate (calcite).

The details of this LTA reaction process were brought to light by the STEM examination of the partially-ashed samples. In general, these samples were simply made up of mixtures of raw coal and fully-ashed particles in varying proportions, based on the amount of ashing time they had seen. However, it was still possible to find individual particles which themselves were only partially ashed.

In such a particle it appears that the fine bassanite network forms continuously as the organic material is burned away and the Ca and S are freed from the matrix. Mineral inclusions originally present in the raw coal particle often remain entrapped within this network as it forms. The bassanite network created thus determines the structure of the low temperature ash of PSOC 98.

It is interesting to speculate on the possible origin of the "gauze" developed by this reaction. It is well known that for coals from the western U.S., organic Ca is readily ion-exchangeable(21). This indicates that the Ca has ready access to the pore structure of the coal. If, during LTA, the Ca in the raw coal reacts in place with the organic S and the oxygen plasma, it could be that the bassanite gauze produced has a network structure related to the pore structure of the raw coal. The 30 nm size of the bassanite crystallites is also comparable to the diameters of a significant portion of the pores likely to be found in coal(22). It may therefore be possible to obtain heretofore unobtainable topographical information of the pore structure of pulverized coal particles by careful LTA experiments. This information would be of great use for modeling the combustion of such particles in commercial boilers. Further work is under way to investigate this possibility.

Although most of the ash produced from PSOC 279 consisted of particles

which appeared to be agglomerates of the mineral inclusions found in the raw coal, some "gauzy" particles were also generated during ashing. In analogy to the results from PSOC 98 just described, this suggests that the gauze was produced from inorganic elements chemically bound in the organic matrix of the starting coal. Unlike the Wyoming coal, however, the coal from Indiana had a matrix that contained primarily Al and Si. This combination of elements has been found by STEM analysis in the matrix of another midwestern coal as well(9). The STEM analysis of the gauzy ash particles for PSOC 279 also showed principally Al and Si. It appears that for this coal, the Al and Si from the organic matrix could react during ashing to produce new crystalline mineral matter. This transformation during LTA has not been previously reported.

The thermochemical modeling of the system indicated that Al and Si should preferentially react together with the oxygen of the LTA plasma to form one or more alumino-silicate compounds, as opposed to the separate formation of alumina and silica. This could not be directly confirmed by electron diffraction in the STEM, for several reasons. First, the mineral inclusion content of the gauzy particles was much higher for this coal than for PSOC 98. In addition, the microprobe results show that nearly 30 percent of these inclusions were alumino-silicates of various types. Selected area diffraction patterns of portions of gauzy particles therefore tended to be quite complex, and not readily amenable to interpretation. An attempt was made to use microdiffraction on the small regions of the network matrix which appeared to be relatively inclusion-free. However, the material was quickly destroyed by the high beam currents involved. The most that can be said from the present work is that STEM microanalysis supports the prediction of the thermochemical model by confirming the combined presence of Al and Si in the matrix of the gauzy ash particles from PSOC 279.

The thermochemical modeling also predicts another LTA transformation for PSOC 279. The modeling results indicate that pyrite is not a stable phase under the low temperature ashing conditions, and is expected to transform to an $\text{Fe}_2(\text{SO}_4)_3$ -type compound. Sulfur is expected to leave the system as SO_3 vapor.

A variety of LTA transformations involving Fe- and S-bearing compounds have been reported previously. Pyrite has been reported as either remaining unchanged(16,25), reacting to form coquimbite and other Fe^{3+} sulfates(17,24,25), or oxidizing to hematite(19). It is generally accepted that rozenite and other Fe^{2+} sulfates oxidize to Fe^{3+} sulfates during LTA(17,23-25). Indeed, in the most recent of these papers it was shown by Mossbauer spectroscopy that, for the LTA conditions used, all of the Fe^{3+} sulfate produced during LTA originated from the Fe^{2+} sulfate in the starting coal, while the pyrite remained unaffected(23).

The STEM results of the present work indicate that a significant amount of pyrite did appear to react during LTA. The pyrite that survived the LTA retains its dense appearance under STEM examination, along with its cubic morphology and high sulfur to iron ratio. By comparison, the

decomposition product has a highly porous structure, a much lower S:Fe ratio, and, in many (but not all) instances, has apparently lost its overall cubic shape. It was difficult to obtain electron diffraction patterns from these latter particles because of their unstable nature under the electron beam. In the few instances where a diffraction pattern was successfully recorded, the best fit for indexing the pattern appeared to be the Fe³⁺ sulfates, coquimbite and para-butlerite. The large proportion of these low S:Fe ratio particles (relative to surviving pyrite particles) observed in the ashed PSOC 279 rules out the possibility of their formation being completely the result of the oxidation of the starting iron sulfates in this coal. Only a very small fraction of the starting mineral matter in the coal was present in the form of Fe²⁺ sulfate.

For the LTA conditions used in the present work, pyrite in the starting coal did partially decompose. This appeared to occur on a particle-by-particle basis; no intermediate reaction products were observed. The rather sporadic nature of the decomposition of pyrite during LTA has been shown previously in tests where pyrites from different sources were subjected to LTA(19). The reason for this behavior is still not known.

One additional prediction of the thermochemical modeling requires comment. SiO₂ is not thermodynamically stable under LTA conditions, but instead should be reacting with other compounds to form aluminosilicates. However, silica particles were still easily identifiable as a specie surviving LTA. There are at least two possible explanations for this. The first is that silica was generally found in relatively large particles, and so was not able to mix intimately with other compounds. Secondly, the kinetics of many reactions may be too slow for them to take place in the time frame of a LTA experiment. As was pointed out earlier, the thermodynamic models assume that equilibrium is reached.

References

1. Walker, P. L., Jr., Spackman, W., Given, P. H., White, E. W., Davis, A., and Jenkins, R. G., "Characterization of Mineral Matter in Coals and Coal Liquefaction Residues", 1st Annual Report to EPRI, Project RP-366-1 (Palo Alto, CA, 1975).
2. Walker, P. L., Jr., Spackman, W., Given, P. H., White, E. W., Davis, A., and Jenkins, R. G., "Characterization of Mineral Matter in Coals and Coal Liquefaction Residues", EPRI AF-417, Project RP-366-1 (Palo Alto, CA, 1977).
3. Lee, R. J., Huggins, F. E., and Huffman, G. P., in Scanning Electron Microscopy/1978/1 (Ed. O. Johari), Scanning Electron Microscopy, Inc. (AMF O'Hare, IL, 1978) p. 561.

4. Huggins, F. E., Kosmack, D. A., Huffman, G. P., and Lee, R. J., in Scanning Electron Microscopy/1980/1 (Ed. O. Johari), Scanning Electron Microscopy, Inc. (AMF O'Hare, IL, 1980) P. 531.
5. Huggins, F. E., Huffman, G. P., and Lee, R. J., in Coal and Coal Products: Analytical Characterization Techniques (Ed. E. L. Fuller, Jr.), ACS Symposium Series, No. 205, ACS (New York, 1977) p. 239.
6. Harris, L. A., Braski, D. N., and Yust, C. S., in Microstructural Science, Vol. 5 (Ed. J. D. Braun, H. W. Arrowsmith, and J. L. McCall), Elsevier North-Holland, Inc. (New York, 1977) p. 351.
7. Hsieh, K. C. and Wert, C. A., Mat. Sci. Eng., 50, 117 (1981).
8. Heinemann, H. in Proceedings of the International Conference on Coal Science, Dusseldorf, 7-9 Sept. 1981, Verlag Gluckauf (Essen, 1981) p. 567.
9. Allen, R. M. and VanderSande, J. B., Fuel, 63, 24 (1984).
10. Erickson, G., Acta Chem. Scand., 25, 2651 (1971).
11. Erickson, G. and Rosen, E., Chemica Scripta, 4, 193 (1973).
12. Erickson, G., Chemica Scripta, 8, 100 (1975).
13. Bessman, T. M., "SOLGASMIX-PV, a Computer Program to Calculate Equilibrium Relationships in Complex Chemical Systems", ORNL/TM-5775, Oak Ridge National Laboratory (1977).
14. JANAF Thermochemical Tables, 2nd edition, Ed. D. R. Stull and H. Prophet, U. S. Dept. of Commerce, National Bureau of Standards Publication NSRDS-NBS 37 (1971).
15. Robie, R. A., Hemingway, B. S., Schafer, C. M., and Haas, J. L., Jr., "Heat Capacity Equations for Minerals at High Temperatures", U.S. Geological Survey Rep. 78-934, U.S. Dept. of the Interior (1978).
16. Gluskoter, H., Fuel, 44, 285 (1965).
17. Mitchell, R. S. and Gluskoter, H. J., Fuel, 55, 90 (1976).
18. Painter, P. C., Coleman, M. M., Jenkins, R. G., Whang, P. W., and Walker, P. L., Jr., Fuel, 57, 337 (1978).
19. Miller, R. N., Yarzab, R. F., and Given, P. H., Fuel, 58, 4 (1979).
20. Morgan, M. E., Jenkins, R. G., and Walker, P. R., Jr., Fuel, 60, 189 (1981).
21. Durie, R. A., Fuel, 40, 407 (1961).

22. Gan, H., Nandi, S. P., and Walker, P. L., Jr., *Fuel*, 51, 272 (1972).
23. Guilianelli, J. L. and Williamson, D. L., *Fuel*, 61, 1267 (1982).
24. Montano, P. A., *Fuel*, 56, 397 (1977).
25. Huggins, F. E. and Huffman, G. P., in *Analytical Methods for Coal and Coal Products*, Vol. III, (Ed. C. Karr, Jr.), Academic Press (New York, 1979) p. 371.

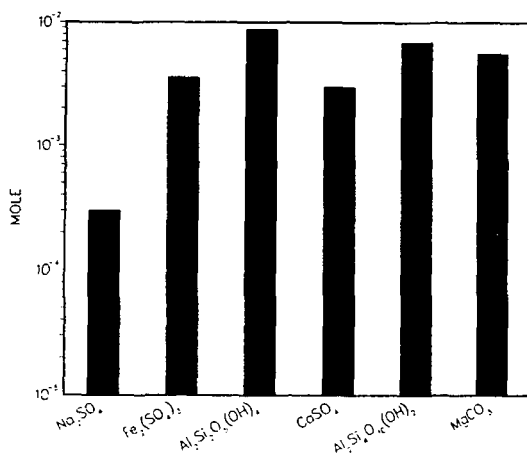


Figure 1 - Thermodynamically stable condensed phase species as predicted by the equilibrium thermochemical modeling. The plot shows the number of moles of each stable species that would be produced after equilibrium was reached under LTA conditions. The starting material was 100 g of PSOC 98.

MINERAL TRANSFORMATIONS DURING ASHING AND SLAGGING OF SELECTED LOW-RANK COALS

S.K. Falcone, H.H. Schobert, D.K. Rindt, and S. Braun

University of North Dakota Energy Research Center
Box 8213, University Station
Grand Forks, North Dakota 58202

Introduction

Inorganic species are incorporated in low-rank coals in many ways: as ion-exchangeable cations, as coordination complexes, and as a diverse array of discrete minerals. In some cases an element will be present in more than one form; potassium, for example, occurs both as an exchangeable cation and in association with clay minerals. The variation in association of inorganics among the multiple modes of occurrence results in a very complex series of reactions and mineral transformations when low-rank coals are ashed or slagged. The behavior or the inorganic components can be at least as important to effective operation as the behavior of the carbonaceous portion in low-rank coal utilization processes. The determination of the extent of the changes in bulk composition and in mineral phases during controlled laboratory ashing is very important in developing an understanding of ash or slag behavior during coal processing and how such changes are related to process conditions.

In the past, mineralogical determinations using ash formed at the standard temperature of 750°C identified minerals which were not originally present in the raw coal but which were artifacts of the ashing procedure. This was due to the alteration of minerals by oxidation, dehydration and other processes at high temperatures. Recent studies by Miller et al (1), Frazer and Belcher (2), and O'Gorman and Walker (3) have concentrated on relating raw coal mineralogy to ash mineralogy generated at low temperatures. Low-temperature ashing (LTA) theoretically would enable one to obtain the true mineralogical composition of a coal since little mineral alteration occurs up to 125°C. Mitchell and Gluskoter (4) expanded this concept to study low to high temperature mineral transformations in ash of subbituminous and bituminous coals. With few exceptions the application of LTA in ash mineralogy studies has been primarily associated with subbituminous and bituminous coals (5). In fact, Miller et al (1) and Frazer and Belcher (2) state that LTA may be unsuitable for obtaining the original mineralogy in lignites without appropriate pretreatment. This is due to the high organic oxygen content with associated inorganic exchangeable cations characteristic of lignites. The presence of organically-bonded inorganics drastically increases the ashing time thereby increasing the chances of mineral alteration by oxidation. In addition, the release of organically-bound cations and organic sulfur in contact with mineral matter can alter the original coal mineralogy with an extended period of low-temperature ashing.

The purpose of this study is to identify mineral transformations in low to high temperature ashes (125°, 750°, and 1000°C) and slags (1300°C) characteristic of lignites. The processes responsible for certain mineral transformation are also examined.

Twelve low-rank coals were selected from the northern Great Plains and Gulf Coast. Nine North Dakota lignites, two Gulf Coast (Texas and Alabama) lignites, and one subbituminous coal from Montana were studied (Table I).

Experimental

The mineral matter composition of each coal sample was determined directly by X-ray diffraction (XRD) of low temperature ash (LTA). A LFE Model 504 four-chamber oxygen

Table I. Location and Inorganic Analyses (XRF) of Coals Studied. All Coals are Lignites Except for Absaloka Subbituminous

Coal Name	Locality	Major and Minor Elements (Percent)									
		Si	Al	Fe	Mg*	Ca	Na*	S	K	Tl	Ba*
+ Absaloka	Big Horn Co., Montana	< 3.5	1.61	2.58	0.08	0.37	0.33	3.92	0.12	0.06	0.03
Beulah Low Sodium	Mercer Co., North Dakota	0.90	0.54	1.02	1.18	1.57	0.14	2.01	0.09	0.05	0.02
Beulah High Sodium	Mercer Co., North Dakota	0.35	0.29	0.52	0.67	1.81	0.46	0.75	ND	0.06	0.04
Center	Oliver Co., North Dakota	0.66	0.44	0.89	0.94	1.70	0.40	0.65	0.08	0.32	0.04
Choctaw	Choctaw, Alabama	1.06	0.49	1.87	0.56	0.84	0.09	2.50	0.10	0.04	ND
Falkirk	McLean Co., North Dakota	0.86	0.50	0.48	0.91	2.60	0.01	0.55	0.15	0.04	0.02
Gascayne Blue	Bowman Co., North Dakota	1.09	0.73	0.25	0.38	2.28	0.27	0.93	0.14	0.05	0.13
Gascayne Red	Bowman Co., North Dakota	2.86	0.87	0.39	0.59	1.74	0.13	1.12	0.13	0.12	0.06
Indian Head	Mercer Co., North Dakota	0.71	0.49	0.68	0.97	1.56	0.62	0.44	0.12	0.04	0.05
Pike	Pike County, Alabama	1.11	0.66	0.36	0.11	1.77	NA	2.28	0.10	0.65	NA
San Miguel	Atascosa Co., Texas	3.58	1.06	0.47	ND	1.20	0.60	1.88	0.35	0.08	NA
Velva	McHenry Co., North Dakota	0.56	0.33	0.26	0.11	0.98	0.09	NA	0.05	0.02	0.03

*Concentrations measured by neutron activation analyses (NAA).

+Absaloka coal analysis completely by NAA.

NA (Not Available) ND (Not Detected)

plasma low temperature asher was used. The ashing procedures used were modified after Miller and Givens' (6) technique for low temperature ashing of subbituminous and bituminous coals. One set of samples was ion-exchanged in 1N ammonium acetate at 70°C for 24 hours and freeze-dried prior to low temperature ashing. This procedure was repeated three times to ensure removal of ion-exchangeable cations. Another, but untreated, sample set was also ashed. Preliminary comparison of sample sets showed the exchanged samples to have reduced ashing time and identical mineralogy except for the presence of bassanite in non-exchanged samples. This difference will be discussed later.

Modifications in operating procedures are as follows: an RF Power of approximately 150W and an oxygen flow of 100cc/min at 2 psi were maintained along with a chamber pressure of 1mm Hg. Samples were stirred once every 2 hours during the first eight hours and every eight hours during the remaining ashing time.

Samples were also ashed at 750°C in accordance with ASTM procedure D3174-73 and will be referred to as ASTM samples (7). Samples were then ashed at 1000°C following the same procedure for 750°C coal ashing and will be referred to as HTA (high temperature ash) samples. Finally raw coal samples were heated to 1300°C forming slag. All slag samples were air quenched.

Mineralogical composition of ash samples was analyzed by XRD. X-ray fluorescence (XRF) analysis was also used for bulk ash analysis. Raw coal analysis was performed by XRF and neutron activation (NAA). XRF elemental analyses of raw coal samples are listed in Table I.

Results and Discussion

Mineralogical phases formed at different temperatures for each coal sample are summarized in Table II. The major mineral phases detected by XRD in LTA samples are quartz, pyrite, bassanite, kaolinite and plagioclase. The processes responsible for mineral transformations include oxidation, vaporization, sulfur fixation, dehydration, solid-state interactions, and recrystallization. The temperatures at which specific transformations occur are based on previous experimental work by Mitchell and Gluskoter (4) and published chemical data in the Handbook of Chemistry and Physics (8). In addition to mineral-mineral interactions it is believed that reactions between minerals and exchangeable cations occur (9).

Pyrite (FeS_2) is present in all LTA samples. While Miller et al (1) stated that pyrite may be oxidized with increased low temperature ashing time in lignites no evidence of oxidized forms of iron was seen by XRD. This may be attributed to the pretreatment of samples with ammonium acetate, thereby reducing ashing times as much as 50%. In ASTM samples pyrite is oxidized to hematite (Fe_2O_3) and magnetite (Fe_3O_4). According to Miller and Gluskoter (4), pyrite oxidizes at 500°C. With the oxidation of pyrite to iron oxide rather than iron sulfate, pyritic sulfur is released. The formation of sodium and calcium sulfates, detected in ASTM ash, may be associated with the release of pyritic sulfur. The source of such sulfates may be the interaction of pyritic sulfur released during pyrite oxidation with carbonates as well as with organically-bound calcium and sodium.

Bassanite ($\text{CaSO}_4 \cdot 0.5\text{H}_2\text{O}$) is present in some of the sample LTAs. Bassanite most likely forms from the dehydration of gypsum ($\text{CaSO}_4 \cdot 2\text{H}_2\text{O}$) at 65°C. Gypsum was detected by scanning electron microscopy (SEM) in raw coal samples. Another source of calcium or sodium sulfate may be the fixation of organic sulfur by organically-bound calcium or sodium cations (9, 10). In this case, bassanite is simply an artifact of the low temperature ashing procedure. This phenomenon is typical of coals having abundant alkali cations associated with carboxyl groups. Continued increases in ashing temperature results in complete dehydration of bassanite to anhydrite (CaSO_4) at 400°C. Anhydrite is a major mineral phase in ASTM and HTA samples and is present in most slags.

Kaolinite ($\text{Al}_2\text{Si}_2\text{O}_5(\text{OH})_4$) is present in only LTA samples. Kaolinite dehydration occurs approximately from 400° to 525°C (4). With removal of water by dehydration, the kaolinite structure collapses, retaining some degree of order forming

Table 11. Mineralogical Composition of Ash and Slag Samples Determined by XRD*

Sample	LTA (~125°C)	ASTM (750°C)	HTA (1000°C)	Slag(1300°C)
Absaloka	Quartz Pyrite Kaolinite Plagioclase Bassanite	Quartz Anhydrite Hematite	Anhydrite Magnetite Hematite Quartz Melilite Plagioclase Nepheline	Plagioclase Hematite Magnetite Quartz
Beulah-Low Sodium	Quartz Pyrite Kaolinite Bassanite	Quartz Hematite Magnetite Anhydrite	Anhydrite Pyroxene Magnetite Hauyne Hematite Quartz	Anhydrite Pyroxene Magnetite
Beulah-High Sodium	Quartz Bassanite Kaolinite Pyrite	Anhydrite Hematite Magnetite Quartz Melilite Hauyne	Anhydrite Melilite Magnetite Hematite Hauyne Quartz Corundum	Melilite Hauyne Nepheline Magnetite Quartz Corundum
Center	Quartz Bassanite Pyrite Kaolinite	Anhydrite Hematite Quartz	Anhydrite Hauyne Pyroxene Melilite Hematite Quartz	
Choctaw	Quartz Pyrite Kaolinite Bassanite Plagioclase	Anhydrite Quartz Hematite Magnetite Plagioclase Pyroxene	Anhydrite Quartz Hematite Quartz Magnetite Plagioclase	
Falkirk	Quartz Kaolinite Pyrite	Anhydrite Quartz Hematite Magnetite Melilite (trace)	Anhydrite Quartz Melilite Hematite Magnetite Hauyne	Melilite (Akermanite) Anhydrite Pyroxene Hematite
Gascoyne Blue- High Sodium	Quartz Kaolinite Pyrite Calcite Sodium Sulfate (trace)	Anhydrite Quartz Hematite Magnetite Nosean Melilite	Anhydrite Melilite Hauyne Quartz	Anhydrite Pyroxene Spinel Melilite Magnetite

Table II. Mineralogical Composition of Ash and Slag Samples Determined by XRD*--
Continued

Sample	LTA (~125°C)	ASTM (750°C)	HTA (1000°C)	Slag(1300°C)
Gascoyne Red- Low Sodium	Quartz Kaolinite Pyrite	Quartz Anhydrite Hematite Magnetite	Quartz Anhydrite Pyroxene Hematite Hauyne	(Amorphous)
Indian Head- High Sodium	Quartz Pyrite Kaolinite Bassanite	Anhydrite Quartz Hematite Nosean Melilite Hauyne Sodium Sulfate (?)	Melilite Hematite Anhydrite Hauyne Magnetite Pyroxene	
Pike	Quartz Pyrite Kaolinite	Anhydrite Quartz Pyrite	Anhydrite Hematite Melilite Anorthite Quartz	
San Miguel	Zeolite (Heulandite) Quartz Kaolinite Pyrite Bassanite Plagioclase	Zeolite Anhydrite Hematite Quartz Plagioclase (Anorthite) Melilite	Plagioclase (Anorthite) Hematite Quartz Magnetite Anhydrite	(Amorphous)

*Minerals listed in decreasing order of peak intensities and occurrence.

metakaolin. No metakaolin was detected by XRD in ASTM samples perhaps due to its poorly defined crystalline structure. However, it is believed that the basic kaolinite components are present in an amorphous form in ASTM ash. With increasing temperature the collapsed kaolinite structure forms corundum ($\gamma\text{-Al}_2\text{O}_3$). While mullite ($3\text{Al}_2\text{O}_3 \cdot 2\text{SiO}_2$) and cristobalite (SiO_2) have been reported to form from well-ordered kaolinites in bituminous coals at 1000°C (4) neither were observed in HTA samples. According to Grim (11), the absence of mullite suggests that the original kaolinitic structure was poorly defined. It has also been suggested by Grim (11) that the presence of impurities in the form of alkali ions, such as in lignites, retards the development of mullites and cristobalite. The mechanism for this is not fully understood.

The collapsed kaolinitic structure acts as a source or framework for several different aluminosilicate complexes formed in HTA and slag samples. Common minerals found are as follows: anorthite ($\text{CaAl}_2\text{Si}_2\text{O}_8$), pyroxenes ($(\text{Ca},\text{Na})(\text{Mg},\text{Fe},\text{Al})(\text{Si},\text{Al})_2\text{O}_6$), melilites ($(\text{Na},\text{Ca})_2(\text{Mg},\text{Fe},\text{Al})(\text{Si},\text{Al})_2\text{O}_7$), haüyne ($(\text{Na},\text{Ca})_{4-8}(\text{AlSiO}_4)(\text{SO}_4)_{1-2}$), nosean ($\text{Na}_3\text{Al}_6\text{Si}_6\text{O}_{24}\text{SO}_4$) and nepheline ($(\text{Na},\text{K})\text{AlSiO}_4$). At 1000°C aluminosilicates minerals form from solid-state reactions of kaolinitic material with cations derived from carbonates, oxides, or sulfates. Interstitial substitution of alkali cations occurs within the dehydrated kaolinite structure with increasing temperature due to thermal expansion. In some coals, particularly those high in sodium, these aluminosilicates are also seen in ASTM samples.

At 1300°C inorganics are in a liquid phase. Upon quenching some sample slags remain amorphous due to rapid cooling thereby inhibiting nucleation of elements preventing the formation of crystalline structures. Other samples recrystallized upon cooling forming previously existing and new aluminosilicate structures. Differences between sample slagging behavior can be traced to silica content of the raw coal. Samples high in silica, such as Gascoyne Red and San Miguel coals, formed amorphous slags upon cooling. Samples having relatively low silica contents such as Absaloka, Beulah High and Low Sodium, Falkirk and Gascoyne Blue coals, formed crystalline slags when cooled. Anhydrite and magnetite are still present at 1300°C .

Minor amounts of calcite (CaCO_3) were detected in raw coal samples by SEM. XRD failed to detect calcite in LTA samples possibly due to extraction by ammonium acetate or because the amounts of calcite were below detection limits ($\sim 5\%$). For the most part, calcium is supplied to the system by gypsum and organically-bound calcium. As previously discussed, calcium whether in the form of bassanite, calcite, or cations in LTA samples forms anhydrite in ASTM samples. In HTA samples calcium reacts primarily with dehydrated kaolinite forming aluminosilicates discussed under kaolinite reactions.

Quartz (SiO_2) is stable throughout the ash samples at varying temperatures up to 1000°C . In slag analysis, quartz is not always present in crystalline form but forms an amorphous substance along with other compounds.

With increasing temperature quartz peak intensities in HTA samples decrease or disappear while various aluminosilicate peaks increase in intensity and number. According to Rindt et al (12) localized reducing areas are present within coal particles during combustion. In these areas, reactions between volatilized sodium and quartz occur forming sodium silicates (13). The sodium is fixed and not readily released on further heating.

Figure 1 displays a typical X-ray diffractogram sequence from LTA sample through slagging of the Beulah High Sodium lignite. Predominant peaks are identified according to the mineral phases present. Mineral transformations at higher temperatures are characterized by the presence of numerous aluminosilicate solid-solution series. Often several members of a particular solid-solution series have almost identical diffractogram patterns making identification by XRD difficult. When comparing several of these diffractograms there is little difference between LTA samples while ASTM, HTA, and slag samples are quite different. When comparing mineralogical differences to raw coal elemental compositions of various coals samples containing higher amounts of sodium tend to form aluminosilicates at lower temperatures (750°C) than samples high in calcium. High sodium coals such as Beulah

High Sodium and Gascoyne Blue develop complex silicates in ASTM samples and are known to be high fouling coals. Typical of such alumino-silicates in ASTM, HTA and slag samples are melilites, hauyne, nepheline, nosean and pyroxenes. Commonly these are minerals found in combustion fouling deposits of most lignites.

Concluding Remarks

The results of this study reflect the preliminary stage of investigation into the mineral phase transformations seen in low-rank coals. The original mineralogies of coals sampled do not vary a great deal. Quartz, kaolinite, pyrite, and bassanite are found in abundance in each LTA sample. Greater differences between samples are apparent at higher temperatures where complex alumino-silicates predominate. Perhaps this is a reflection of differences not so much in original mineral matter but in the total inorganic composition of the coal, specifically the presence of exchangeable alkali cations. The interactions of such organically-bound cations with crystalline inorganic phases in lignites account for differences in ashing and slagging behavior between coal samples (9).

The processes responsible for most reactions identified are oxidation, dehydration, sulfur fixation, solid-state interactions, vaporization, and recrystallization. Isolating specific reactions occurring in a multi-component system is difficult at best. Understanding the thermodynamics of mineral transformations is a necessity and will be pursued in future study. In addition, future studies isolating mineral pairs to observe phase transformations at various temperatures will support or refute results presented here.

Literature Cited

1. Miller, R.N.; Yarzab, R.F.: and Given, Peter. Fuel 1979, 58, 4.
2. Frazer, F.W.; and Belcher, C.B. Fuel 1973, 52,41.
3. O'Gorman, J.V.: and Walker, P.L. Fuel 1973, 52,71.
4. Mitchell, R.S.; and Gluskoter, H.J. Fuel 1976, 55,90.
5. Gluskoter, J.J. Fuel 1965, 44, 285.
6. Miller, R.N.; and Given, Peter. 'A Geochemical Study of the Inorganic Constituents in Some Low-Rank Coals' Technical Report, Pennsylvania State University to the U.S. Department of Energy, Rep. FE-2494-TR-1, 1978.
7. Annual Book of American Society of Testing Materials Standards 1979, Part 26: Gaseous Fuels; Coal and Coke; Atmospheric Analysis.
8. Handbook of Chemistry and Physics 54th edition, Chemical Rubber Company, 1973.
9. Morgan, M.E.; Jenkins, R.G.; and Walker, P.L. Jr. Fuel 1981, 60, 189.
10. Painter, P.C.; Coleman, M.M.; Jenkins, R.G.; and Walker, P.L. Jr. Fuel 1978, 57, 125.
11. Grim, R.E. Clay Mineralogy, McGraw-Hill, New York, 1968, Chapter 9.
12. Rindt, D.K.: Selle, S.J.; and Beckering, W. 1979 American Society of Mechanical Engineers, Corrosion and Deposits Division, Reprint 79-WA/CS-5.
13. Boow, J. Fuel 1972, 51, 170.

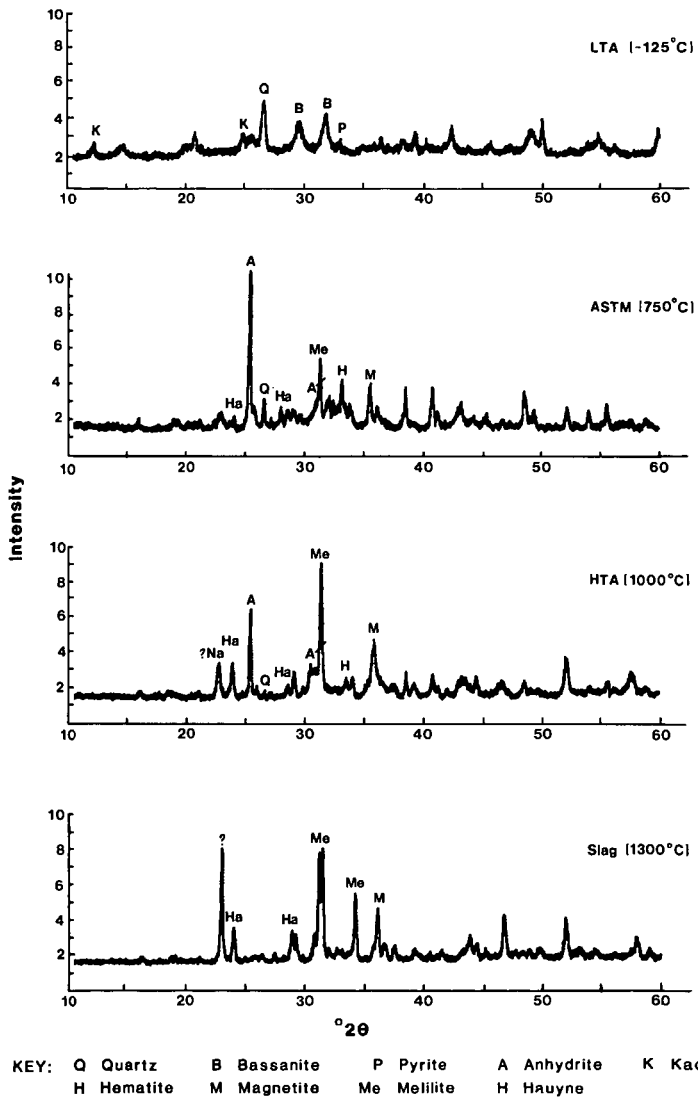


Figure 1. X-ray diffractograms of LTA, ASTM, HTA, and slag samples of Beulah high sodium coal.

HIGH TEMPERATURE INTERACTIONS AMONG MINERALS OCCURRING IN COAL

BY
DONALD L. BIGGS AND CURTIS G. LINDSAY

AMES LABORATORY*, IOWA STATE MINING AND MINERAL
RESOURCES RESEARCH INSTITUTE, AND
THE DEPARTMENT OF EARTH SCIENCES,
IOWA STATE UNIVERSITY
AMES, IOWA 50011

INTRODUCTION

Mineral impurities in coal are known to be primary contributors to the slagging and fouling of utility boilers, fly ash and bottom ash production as well as atmospheric pollution. They also produce undesirable effects in some parts of hydrogenation processes such as liquifaction and gasification (1,2,3). Despite a long history of investigation prompted by these observations, many questions remain unanswered.

Simple empirical relationships between fusion temperature of the furnace deposits and the mineralogy of coals have been proposed (4,5,6). More recently attempts have concentrated on a physico-chemical view of the problem comparing ash fusion temperatures with phase relations in three-component chemical systems (7,8). This method of attack has yielded some significant results, but at least some researchers (8) have questioned the assumption that these processes occur under conditions of equilibrium.

The aim of the research described here is to observe interactions between minerals known to occur in coals in the most direct fashion possible and in the simplest conditions consistent with causing the reactions to occur. It is considered that observation of simple mixtures of minerals observed to enter into reaction may make possible a better accounting of the processes by which slag and fouling deposits form in furnaces.

EXPERIMENTAL METHODS

ISOLATION AND IDENTIFICATION OF COAL MINERALS. Two coal samples collected from different coal basins in the United States (see Table I), were subjected to low-temperature ashing as described by Gluskoter (9). This process avoids destruction of the minerals while oxidizing the organic portion of the coal. This ashing procedure occurs at a much lower temperature than that of the American Society for Testing and Materials (ASTM) method it is given the name of "low-temperature ash" and generally abbreviated, LTA. In formation of a mineral concentrate by low-temperature ashing (LTA) a few changes are anticipated; some clays are reversibly dehydrated, hydrated sulfates are reduced to the hemihydrate form, for instance gypsum is converted to bassanite. Because these changes are known in advance, due allowance can be made for them.

*Operated for the U. S. Dept. of Energy by Iowa State Univ. under contract No. W-7405 Eng-82.

TABLE I

Coal Samples, Localities of Origin, and Analyses
(all samples run-of-mine)

Seam: Illinois #6
Locality: St. Clair County, Illinois

Analysis:

	9 mesh x 0 Raw	9 x 32 mesh Float	9 x 32 mesh Sink
Moisture (%):	5.31	5.44	2.55
Ash, ASTM (%):	32.86	7.10	68.05
Pyritic Sulfur (%):	2.46	0.76	5.08
Total Sulfur (%):	4.57	4.57	5.94
Heating Value (BTU/lb.):	9,039	13,248	3,574

Seam: Upper Freeport
Locality: Grant County, West Virginia

Analysis:

	9 mesh x 0 Raw	9 x 32 mesh Float	9 x 32 mesh Sink
Moisture (%):	0.30	0.68	0.93
Ash, ASTM (%):	35.90	7.26	72.10
Pyritic Sulfur (%):	1.58	0.27	2.62
Total Sulfur (%):	2.18	1.06	3.00
Heating Value (BTU/lb.):	9,695	13,365	3,086

Mineral constituents of the LTA concentrates were identified by x-ray diffraction techniques. Illite, kaolinite, quartz and pyrite are ubiquitous in the mineral suites; calcite occurs in most concentrates. Many other minerals have been identified in coals, but were not observed in these specimens.

HEATING-STAGE MICROSCOPIC OBSERVATIONS. Following the characterization of the mineral suites by x-ray diffraction techniques, each LTA concentrate was heated in a heating stage mounted on a microscope fitted for observation in vertically incident light. Concentrates examined in this way and the product phases are found in Table II.

TABLE II

LTA Samples and Heating Products

<u>LTA Sample</u>	<u>T_{max} (°C)</u>	<u>Phases Identified</u>
Upper Freeport raw	560	quartz, illite, pyrrhotite
	1410	quartz, mullite ^a
Upper Freeport 1.40 float	1031	quartz ^b
	1250	quartz ^b
Upper Freeport 1.40 sink	635	quartz, illite, pyrrhotite
	1150	quartz, pyrrhotite, illite ^c
Illinois #6 raw	880 ^d	quartz, illite, pyrr- hotite, oldhamite(?)
Illinois #6 1.40 float	625	quartz, illite, pyrr- hotite, troilite (?)
	1370	quartz, pyrrhotite
Illinois #6 1.40 sink	920	quartz, illite, pyrr- hotite, oldhamite
	1334	quartz, pyrrhotite, oldhamite

NOTES:

- ^aXRD peaks occurred at the correct diffraction angles for mulite, but were too weak to permit accurate intensity comparisons.
- ^bThe overall pattern was similar to the one for the illite-kaolinite pair heated to 1410°C, except that stronger peaks for quartz were found in the LTA XRD pattern.
- ^cPeaks were detected at some of the diffraction angles for illite, but the intensities were not comparable with standard patterns; it is possible that these were relict peaks of illite as it began to alter.
- ^dAnother sample of Illinois #6 raw LTA was heated to 1421°C; it formed a hard, dark-coloured glass at about 1400°C, and this material could not be removed from the heating-stage crucible.

The heating stage is limited to inert atmosphere or vacuum operation. Therefore, reactions sensitive to atmospheric conditions, such as partial pressure of oxygen cannot be studied. Furthermore, the extremely small particle size of the sample resulted in inability to observe changes occurring below the mount surface, and to resolve the specific minerals entering into a reaction at any point in the run.

These difficulties were met by obtaining samples of the minerals identified in the LTA concentrate before heating, grinding them to approximately the same size consist as the concentrate, and mounting them in separate domains in the heating stage crucible. The geometry of these mounts is shown in Fig. 1.

EXPERIMENTS WITH KNOWN MINERALS

EXPERIMENTS WITH INDIVIDUAL MINERALS. Single mineral mounts in the heating-stage crucible yielded the expected products, that is, pyrite yielded pyrrhotite and troilite, calcite gave lime and carbon dioxide, and clays reacted under high temperature conditions to yield a silicate glass.

EXPERIMENTS WITH PAIRS AND TRIPLETS OF KNOWN MINERALS. In these experiments, known minerals were ground and placed in the heating-stage crucible in separate domains as pairs or triplets of minerals. The pairs and triplets were heated and the behavior at their boundaries observed. Table III lists the minerals used in pair mounts and the reaction products obtained by heating.

TABLE III

Mineral Pairs and Heating Products

<u>Mineral Pair</u>	<u>t_{max} (°C)</u>	<u>Products Identified^a</u>
calcite-illite	1310	lime (CaO)
calcite-kaolinite	1322	lime (CaO)
calcite-montmorillonite	1285	(indeterminate) ^b
calcite-pyrite	1253	lime, pyrrhotite (Fe _{1-x} S), oldhamite (CaS)
calcite-quartz	1467	quartz (SiO ₂), lime (CaO)
illite-kaolinite	1410	mullite (Al ₆ Si ₂ O ₁₃) ^c
illite-montmorillonite	662	(indeterminate) ^b
illite-montmorillonite	1212	(indeterminate) ^b
illite-pyrite	1519	pyrrhotite, troilite (FeS)
illite-quartz	1450	quartz
kaolinite-montmorillonite	1403	mullite (poorly- crystalline) ^c
kaolinite-pyrite	1445	mullite
kaolinite-quartz	1220	quartz
montmorillonite-pyrite	1053	(indeterminate)
montmorillonite-quartz	1492	quartz
pyrite-quartz	1571	quartz

Notes:

^a Only those products are listed which could be positively identified by XRD; no attempt is made here to deduce the composition of amorphous products.

^b XRD patterns for these heating products did not match any standard pattern closely; attempts to match with computer routines produced results of low reliability.

^c "Poorly crystalline" means that diffraction maxima were found corresponding to the indicated phase, but peaks were not sharp and did not have the correct relative intensities in all cases.

Because the most reactive phases found in the experiments with pairs of minerals were clays, calcite, and pyrite, these were prepared in triplet mounts. In trials using either montmorillonite or illite with calcite and pyrite, a liquid formed at the mutual boundary of the latter pair at 600 - 650°C. Pyrite and calcite had, of course, previously reacted and this liquid therefore occurred between the product phases pyrrhotite and lime. Subsequent x-ray analysis showed the presence of pyrrhotite, lime, and oldhamite. In both instances, the temperature of this reaction was lower than that obtained in the pair mount of calcite and pyrite, 1140°C. When kaolinite was in the mount with calcite and pyrite, the same reaction occurred at 750 - 760°C. Though the fluxing action of the clays is not presently understood, the differences in reaction temperature with and without clay is considered significant.

The most obvious reaction of the clays themselves during these experiments was a darkening beginning with pyrite decomposition. This was more marked in the case of illite and montmorillonite. It is considered that in all cases, the clay mineral present formed a silicate glass, much like those found in furnace slags, but having, perhaps, less oxygen.

SUPPORTING EXPERIMENTS. To examine the effect of oxidizing and reducing atmosphere on these materials, graphite crucibles 10mm in diameter and 5mm deep were packed in the same manner described above and heated in a furnace fitted to permit introduction of controlled gases during heating. After heating, the samples were examined by scanning electron microscopy and energy dispersive x-ray spectroscopy (SEM/EDS). Samples treated in this way are listed in Table IV.

TABLE IV

Subjects of Supporting Experiments

<u>Assemblage</u>	<u>Atmosphere</u>	<u>T (°C)</u>	<u>Duration (min)</u>
calcite-kaolinite	inert	1400	60
calcite-quartz	inert	1400	60
pyrite-quartz	oxidizing	1200	30
pyrite-quartz	reducing	1200	30
pyrite-calcite	reducing	1200	30
pyrite-kaolinite	oxidizing	1200	30
pyrite-kaolinite	reducing	1200	30
pyrite-montmorillonite	inert	800	15
pyrite-montmorillonite	reducing	800	15
py.-calc.-kao.	reducing	1200	30
py.-calc.-mont.	inert	800	15
py.-calc.-mont.	reducing	800	15

NOTE:

The indicated temperature was the steady-state temperature for the trial. The indicated duration was the period of time for which that steady-state temperature was maintained.

In all these cases where pyrite was used with a clay, iron was found to have migrated from the region that was originally iron sulfide into the clay. Elemental mapping showed the presence of iron to have completely pervaded the region formerly occupied by clay. In the calcite-pyrite pair mount, the iron was lost. EDS mapping showed the presence of abundant calcium and sulfur, but iron was present in small amount. In all mounts containing calcite and pyrite, the calcium and sulfur peaks were present in the region originally occupied by calcite, and sometimes found in the region that had been pyrite-filled.

SUMMARY AND CONCLUSIONS

It is apparent that the phenomena described here are not complete processes terminating in equilibrium assemblages. The times of reaction are too short for many of the products of silicates such as clays and quartz to come to thermodynamic equilibrium at the new temperature. That this is indeed the case in operation of power-plant boilers is obvious from the consideration of the amount of glass found in furnace slags and fly-ash.

Illite and montmorillonite are similar in structure and differ slightly from kaolinite in this regard. The first two are composed of two silicon-oxygen layers per octahedral layer containing iron, magnesium and aluminum and in kaolinite the ratio of tetrahedral and octahedral layers is 1. In these crystals, thermal modification is easier because the bonds formed between the Al, Fe, and Mg atoms and oxygen are weaker than the Si-O bonds. Clays, therefore are expected to be more reactive than the silica crystals. There is evidence that some glass is formed in the clay mineral domains during thermal treatment and that iron diffuses into the mass. Further inquiries are in progress to answer these questions.

Calcite appears largely inert until temperatures approaching 600°C in the presence of some of the clay minerals and inert until about 900°C in their absence. The cause of this fluxing is not well understood at this time, but investigations are planned to elucidate this behavior. At whatever temperature, the reaction observed is for the calcite to decompose to lime (CaO) and carbon dioxide. The extent to which carbon dioxide fluxes further reaction is not known, but must be considered as an important step in complete explanation.

Like calcite, pyrite is quite reactive and its thermal behavior is influenced by the presence of clay minerals. The initial reaction temperature of pyrite alone or in the presence of calcite alone is to produce pyrrhotite, (Fe_{1-x}S) and at the highest temperature, troilite (FeS). The loss of sulfur is obvious and continues over an appreciable temperature range. T

The most important reaction products are those of the iron enrichment of the clay minerals, probably a precursor of the iron oxide and glass mixtures commonly observed in slags and fly-ashes, and the formation of the sulfide of calcium, oldhamite. That oldhamite is observed in all experiments where calcite and pyrite interact, and that anhydrite is observed only where they have reacted in the presence of an oxygen-rich atmosphere supports the conclusion that oldhamite, formed in the reducing part of a flame, is a necessary precursor to the formation of the sulfate, anhydrite.

Acknowledgements

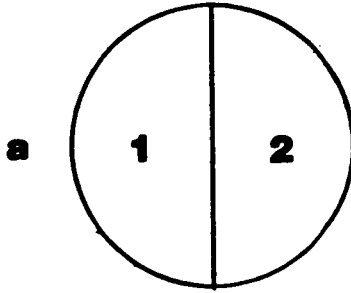
This material is based, in part, on work supported by the U.S. Bureau of Mines, Department of the Interior, under Grant No. G1106002. Any opinions, findings, and conclusions or recommendations expressed in this publication are those of the authors and do not necessarily reflect the views of the U.S. Bureau of Mines, Department of the Interior.

Work on other parts of this publication was performed in Ames Laboratory and was supported by the Assistant Secretary of Fossil Energy, Division of Coal Utilization through the Pittsburgh Energy Technology Center, Coal Preparation Branch.

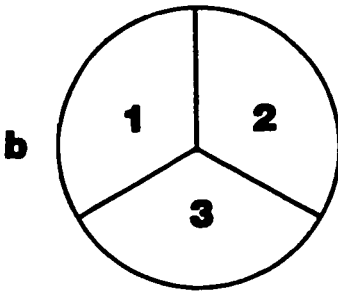
REFERENCES

- (1) Mukkherjee, D.K., and Chowdhury, B. : Fuel, 55, pp.4-8 (1976).
- (2) Wakely, L.D., Davis, A., Jenkins, R.G., Mitchell, G.D., and Walker, P.L. Jr. : Fuel, 58, pp.379-385 (1979).
- (3) Gray, D. : Fuel, 57, pp.213-216 (1978).
- (4) Moody, A.H., and Langhan, D.D. : Combustion, 6, pp.13-20 (1935)
- (5) Gauger, A.W. : Procedures of the American Society of Testing Materials 37, Part I, pp.376-401 (1937).
- (6) Palmenburg, O.W. : Industrial and Engineering Chemistry, 31, pp. 1058-1059. (1939).
- (7) Electric Power Research Institute (EPRI) Report CS-1418, Research Project 736; prepared by Battelle, Columbus Laboratories (1980).
- (8) Huggins, F.E., Kosmack, D.A., and Huffman, G.P. : Fuel, 60, pp. 577-584 (1981).
- (9) Gluskoter, H.J. : Fuel, 44, pp. 285-291 (1965)

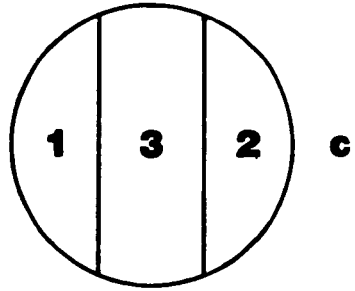
Pair Mounts



Triplet Mounts



**Triple-Junction
Mount**



**Parallel-Boundary
Mount**

Figure 1. Geometric arrangements of mineral pairs and triplets used in heating-stage microscopic experiments and in supporting experiments. Approximate diameters of actual mounts: for heating-stage experiments--5 mm; for supporting experiments--11 mm. In all triplet mounts, mineral "3" was a clay mineral.

FLAME VITRIFICATION AND SINTERING CHARACTERISTICS OF SILICATE ASH

ERICH RAASK

Technical Planning and Research Division of Central Electricity Generating Board,
Kelvin Avenue, Leatherhead, Surrey, UK

The silicate species constitute the bulk of the mineral matter in most coals, and the formation of boiler deposits depends largely on the physical and pyrochemical changes of the ash residue constituents. In this work the mode of occurrence of coal silicate minerals, and the flame induced vitrification and sodium initiated sintering mechanisms have been studied. The pulverized coal flame temperature is sufficiently high to vitrify the quartz particles. On cooling some devitrification occurs and the rate of sintering depends largely on the ratio of glassy phase to crystalline species in the ash. The flame volatile sodium captured by the vitrified silicate particles can initiate the coalescence of deposited ash by viscous flow and the rate of sintering is markedly increased by the alkali-metal dissolved in the glassy phase.

The flame imprinted characteristics of pulverized coal ash relevant to boiler slagging, corrosion and erosion have been discussed previously (1,2). The silicate minerals constitute between 60 and 90 per cent of ash in most coals and boiler deposits are largely made up from the silicious impurity constituents. This work sets out first to examine the mode of occurrence of the silicate mineral species in coal followed by a characterization assessment of the flame vitrified and sodium enriched silicate ash particles. The ash sintering studies are limited to investigations of the role of sodium in initiating and sustaining the bond forming reactions leading to the formation of boiler deposits.

SILICA (QUARTZ) AND SILICATE MINERAL SPECIES IN COAL

The quartz and aluminosilicate species found in most coals constitute the bulk of combustion ash residue. The aluminosilicates include muscovite and illite which contain potassium, and kaolinite species (3,4,5,6). The silica (SiO_2) and alumina (Al_2O_3) as determined by chemical analysis are present in aluminosilicates on an average weight ratio of 1.5 to 1 as reported by Dixon et al. (6). The excess of silica represents the amount of quartz in coal mineral matter:

$$(\text{SiO}_2)_q = (\text{SiO}_2)_t - 1.5(\text{Al}_2\text{O}_3) \quad 1)$$

Where $(\text{SiO}_2)_q$, $(\text{SiO}_2)_t$ and (Al_2O_3) denote respectively the quartz, total silica and alumina contents of ash.

An approximate amount of potassium aluminosilicates in coal mineral matter can be obtained from the potassium oxide (K_2O) content of ash. The amount of non-silicate potassium species is small in most coals and the silicate minerals contain on average 11 per cent K_2O by weight (6). Thus the potassium aluminosilicate content of coal mineral matter ($K_{\text{AL-SIL}}$) by weight per cent is:

$$K_{\text{AL-SIL}} = \frac{\text{K}_2\text{O}}{0.11} = 9.1 \text{ K}_2\text{O} \quad 2)$$

where K_2O denotes the potassium oxide content of ash.

The total amount of silicate minerals equals approximately the sum of SiO_2 , Al_2O_3 and K_2O in ash, and an estimate of kaolinite species is thus given by:

$$\text{Kaolinite} = (\text{SiO}_2 + \text{Al}_2\text{O}_3 + \text{K}_2\text{O}) - (\text{Quartz} + \text{Potassium Silicates})$$

3)

Table 1 gives the SiO_2 , Al_2O_3 and K_2O contents of some US and British bituminous coal ashes (4,7) which were used to calculate the approximate amounts of quartz, potassium aluminosilicate and kaolinite species in the mineral matter.

Table 1: Silicate Species in Mineral Matter of British and US Bituminous Coals

Type of Coal		Ash Constituents, Weight Per Cent of Ash			Mineral Species, Weight Per Cent of the the Total		
		SiO_2	Al_2O_3	K_2O	Quartz	Pot. Alum. Silicates	Kaolinite
Low Silica	British	31.1	18.1	1.2	3.9	10.9	26.2
	US	29.2	14.2	1.5	7.9	13.6	23.6
Medium Silica	British	46.5	22.8	2.8	12.3	25.5	34.3
	US	46.6	27.8	1.1	4.9	10.0	60.6
High Silica	British	55.5	30.0	2.7	10.5	24.5	53.2
	US	56.5	32.2	2.6	8.0	23.6	59.7

Table 1 shows that the kaolinite species constitutes up to 60 per cent of the coal mineral matter. The amount of potassium aluminosilicates, chiefly muscovite and illite is between 10 and 25 per cent, and the quartz content is usually below 12 per cent. The aluminosilicate minerals contain frequently iron, calcium, magnesium and sodium as part replacement for potassium and partly incorporated in the kaolinite structure. Also, the silicate minerals occur as hydrated species with the inherent water content of between 2 to 5 per cent, thus the silicious mineral contents are likely to be about 5 per cent higher than those given in Table 1.

The silica and alumina contents of the first two samples are exceptionally low for bituminous coal ashes. The usual concentration range of silica is 35 to 55 per cent and that of alumina is 20 to 30 per cent thus the aluminosilicate species together with quartz constitute between 60 to 90 per cent of the bituminous coal mineral matter.

The silicate species occur in coal chiefly as separate strata and large particle inclusions, and this mode of occurrence is termed the "adventitious" mineral matter. Fig. 1a shows a typical sample of the adventitious silicate mineral particles, density separated from pulverized coal. The density separation technique does not remove the small silicate particles, chiefly aluminosilicate species dispersed in the coal substance (Fig. 1b). The average ash content of bituminous coals utilized in electricity generating power stations is usually between 12 and 20 per cent (4,8) and about one quarter, 3 to 5 per cent fraction is present as the inherent ash.

The mineral elements can be held in the coal substance as organo-metal salts, and also as a result of molecular adsorption and co-valent bonding. The mineral species dissolved in coal pore water, chiefly chlorides can also be considered as a part of the inherent mineral matter. The lignites and sub-bituminous coals can have a high fraction of the mineral elements, chiefly sodium, calcium and also aluminium and iron chemically combined in the fuel substance (9,10). The chemical reactivity and porosity of the fuel matrix decreases with the increase of coal age from lignite to bituminous rank. The loss of carboxyl, hydroxyl and quinone bonding sites in the fuel matrix results in a low "chemical" mineral matter content of bituminous coals.

CHLORIDE IN COAL PORE AND SEAM WATER

Chloride minerals are rarely found in coal in the form of solid species because of high solubility of sodium, calcium and trace metal chlorides in coal strata waters. The "inherent" water content of coal is related to its porosity and thus the moisture content of lignite deposits can exceed 40 per cent decreasing to below 5 per cent in fully matured bituminous coals (11). Chlorides, chiefly associated with sodium and calcium constitute the bulk of water-soluble matter in British bituminous coals (12) and Skipsay (13) has found that the distribution of chlorine coals was closely related to the salinity of mine waters. Hypersaline brines with concentrations of dissolved solids up to 200 kg m⁻³ occur in several of the British coalfields.

The mode of formation of hypersaline brines has been discussed by Dunham (14) concluding that the connate waters were of marine origin formed by the osmotic filtration through clay and shale deposits. The salinity of the brine ground waters increases with depth and when they are in contact with fuel bearing strata, correspondingly more chloride is taken up by the fuel. However, according to Skipsey (13) the high rank bituminous coals because of their low porosity are unable to take up large amounts of the chloride and associated cations, and the chlorine content rarely exceeds 0.2 per cent. The chlorine content of low rank bituminous coals can reach one per cent and correspondingly the sodium fraction associated with chlorine will amount up to 0.4 per cent of coal. That is, the ash from a high chlorine coal can contain up to 3 per cent of flame volatile sodium. The chlorine content of lignites and sub-bituminous coals is usually low, below 0.1 per cent, and sodium is held chiefly in the fuel substance in the form of organo-metal components (9,10).

All coals contain some sodium combined in the aluminosilicate species which will remain largely involatile in the flame. The ratio of the silicate sodium to non-silicate sodium varies over a wide range. The alkali-metal is present chiefly in the silicates in low chlorine bituminous coals, but in the high chlorine bituminous coals and in many lignites and sub-bituminous coals it is present mainly in a flame volatile form.

FLAME VITRIFICATION OF SILICA MINERALS

A characteristic feature of flame heated ash is that the particles are spherical in shape as shown in Fig. 2. The transformation of the angular silicate mineral particles in pulverized coal to spherical particle ash is a result of the surface tension force acting on the vitrified species. The stress (f) on a non-spherical surface section of the particle is:

$$f = 2\gamma/\rho \quad (4)$$

where γ is the surface tension of glassy silicate and ρ is the radius of curvature. It is evident from equation (4) that the stress is inversely proportional to the radius of curvature and thus the small sharp-edged particles are first to take a spherical form.

Frenkel (15) has shown that time (t) required to transform an angular particle to sphere is given to first approximation by:

$$r = r_0 e^{-t/z} \quad 5)$$

where

$$z = 4\pi\eta r_0 / \gamma \quad 6)$$

and r is the distance of a point on the original surface from the center of a sphere of equivalent volume having radius r_0 , η is the viscosity and γ is the surface tension.

Equation 5 can be used to calculate the approximate time required for a particle to assume a spherical shape when the surface tension, viscosity, size and initial shape of particle are known. Alternatively, an estimate of the viscosity for the change to take place, can be made when the residence time of particles at a given temperature is known. Table 1 gives the calculated values of viscosity when the time for the change is one second. It was assumed that the thickness of moving surface layer was about ten per cent of the radius, and the surface tension of fused ash was taken to be 0.32 N m^{-1} as measured previously (16).

Table 2: Calculated Viscosities for Spheridization of Different Size

Silicate Particles					
Particle Radius, μm	0.01	0.1	1	10	100
Viscosity, N s m^{-2}	2.5×10^7	2.5×10^6	2.5×10^5	2.5×10^4	2.3×10^3

Table 2 shows that the small irregularly shaped particles transform to spheres in a coal flame when the viscosity of the material is several orders higher than that required for bulk flow under gravity, which is about 25 N s m^{-2} . A laboratory technique was used to determine the minimum temperature at which coal mineral species are transformed to spherical shapes (17). Particles of 10 to 200 μm in diameter were introduced into a gas stream and then passed through a vertical furnace. The temperature of the furnace was varied from 1175 to 2025 K and was measured by a radiation pyrometer and by thermocouples placed in the furnace. The residence time of particles in the furnace was between 0.2 and 0.5 sec. depending on the particle size.

Fig. 3a shows a surface-fused silicate particle heated to a temperature some 25 K lower than that required for its spheridization. Fig. 3b shows a spheridized particle heated in the laboratory furnace. Fig. 4 shows the temperature range at which the shape change of different coal mineral particles occurred. The chlorite mineral contain some quartz and the two species spheridized at markedly different temperatures as shown by curves D_1 and D_2 .

The temperature of mineral particles in the pulverized coal flame exceeds 1800 K (Fig. 5), and it is therefore to be expected that all particles with the exception of large size quartz will vitrify and change to spherical shapes. Fig. 6a shows a surface-fused but non-spherical quartz particle found in a sample of fly ash captured in the electrical precipitator. Occasionally ellipsoidal particles of aluminosilicates (Fig. 6b) can be found in the ash indicating that the high temperature residence time was slightly too short for complete spheridization. However, the majority of the ash particles appear to be spherical as shown in Fig. 2.

The spherical silicate ash particles, when viewed at close-up range appear to host a large number of sub-micron particles at the surface (Fig. 6c). The microoids could be silicate crystalloids precipitated from the vitrified phase or sulphate fume particles formed from the non-silicate coal minerals (18). The latter are soluble in a dilute acid (HCl) solution and Fig. 6d shows the acid etched particles. Clearly, most of the microid particles were dissolved and the leach solution contained sodium and potassium sulphates.

Another diagnostic test for silicate ash is to treat the particles with hydrofluoric (HF) acid solution (18,19,20). The acid will dissolve the glassy phase revealing skeletons of crystalline species which may be in the form of mullite needles (Fig. 6e) or quartz crystalloids (Fig. 6f). The ratio of the glassy phase to crystalline species varies from particle to particle depending on the original composition of the silicate minerals, the capture of volatile sodium and the rate of cooling of the flue gas borne ash.

The flame imprinted characteristics of silicate mineral species from the point of view of subsequent sintering are summarized in Table 3.

Table 3: Flame Vitrification and Recrystallization of Silicates

Constituent Species	Particle Vitrification		Recrystallization Tendency	Glass Content
	Temperature Range, K	Extent		
Quartz	1700 to 1900	Medium	Low	Medium
Kaolinite	1600 to 1700	High	High	Medium
Potassium Alumino-silicates	1400 to 1600	High	Low	High

The relative amount of coal mineral quartz surviving in the pulverized fuel flame depends on the particle size and temperature. In the intense combustion of cyclone fired boilers the flame temperature exceeds 2000 K and the quartz particles of all sizes will vitrify. Some quartz particles in the crystalline form will survive the flame treatment in pulverized coal fired boilers and the ash may contain 25 per cent of the original coal quartz in the crystalline form (21).

The kaolinite mineral species in coal contain some sodium, calcium and iron in the crystalline structure (6) and the presence of fluxing metals enhances vitrification of the flame heated particles. The high temperature crystalline form of kaolinite species is mullite and the characteristic needle shapes of mullite (Fig. 6e) are frequently found in large, above 5 μm diameter particles. The mullite needle crystals in ash are always embedded in a glassy phase of the large particles and it appears that the small, below 5 μm diameter particles of the flame heated kaolinite species are not extensively recrystallized on cooling. The crystalline species of illite and muscovite are not found in the flame heated ash and thus it is likely that the potassium alumino-silicates remain on cooling largely in the form of glassy particles.

The inherent silicate ash (Fig. 1b) will coalesce on combustion first to a sintered matrix inside the burning coal particle and also to small slag globules at the surface of coke residue. Fig. 7a shows the slag globules on a coke particle separated from pulverized coal ash and Fig. 7b shows a lace skeleton of sintered ash in another coke particle revealed after combustion at 900 K.

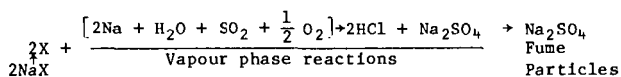
During combustion of the mineral rich coal particles in the pulverized fuel flame ash envelopes may be created which can take the form of cenospheres as shown in Fig. 7c and d. The gas bubble evolution leading to cenosphere formation has been discussed previously (16,22) and the fly ash usually contains between 0.1 and 2 per cent by weight of the lightweight ash. The mineral rich coal particles may leave the combustion ash residue also in the form of plerosphere (spheres-inside-sphere) as shown in Fig. 7e.

The above examples show that the inherent silica ash particles undergo extensive coalescence by sintering and slagging during combustion of the host coal particles. However, the adventitious ash retain the particle identity in the flame and the processes of sintering and slagging take place after deposition on boiler tubes.

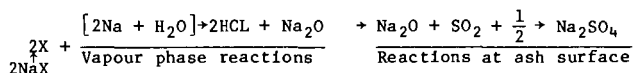
TRANSFER OF FLAME VOLATILE SODIUM TO SILICATES.

The coal sodium originally present as chloride or organo-metal compounds is rapidly volatilized in the pulverized coal flame (23). Subsequently the volatile species are partly dissolved in the surface layer of flame heated silicate particles and partly sulphated in the flue gas (8). The formation of sodium sulphate can proceed via two routes:

Route 1 - In the Flue Gas



Route 2 - At the Surface of Ash Particles



Route 1 for genesis of sodium sulphate fume can be described as the non-captive formation and route 2 as the captive formation.

Some potassium sulphate can also be formed via the two routes. Potassium is present in coal chiefly in the form of potassium aluminosilicates (Table 1) and a large part of the alkali-metal will remain involatile in the flame heated silicate particles. Some 5 to 20 per cent of the potassium is released for sulphation (24) which takes place partly at the surface of the parent particles (25) and partly via the volatilization routes as described above. However, sodium sulphate content of fly ash and chimney content of fly ash and chimney solids is always higher than that of potassium sulphate.

The distribution of the flame volatile sodium between the ash silicate and sulphate phases is markedly influenced by the temperature and residence time of the ash particles in the flame. The high temperature of large boiler flame reduces the viscosity of vitrified silicate particles and as a result a large fraction of the volatile sodium is dissolved in the silicate phase. On average 60 per cent of the sodium is dissolved in the silicate ash particles (6) the remainder being present as sulphate fume particles in the flue gas (20).

THE MECHANISM AND MEASUREMENTS OF SODIUM ENHANCED SINTERING

The formation of sintered ash deposits on boiler tubes requires first a close, molecular distance contact between the particles followed by a growth of particle-to-particle bridges chiefly by viscous flow. Sodium sulphate phase together with some potassium sulphate may play a significant role in the initial stage of sintering by bringing the silicate particles together as a result of surface tension. Sodium sulphate melts at 1157 K but mixed alkali-metal sulphates can form a molten phase at lower temperatures (26).

Once the close contact between the silicate particles has been established a viscous flow of the particle surface layer can commence and the sinter bonds are established according to Equation 7 as discussed by Frenkel (15):

$$\frac{x^2}{r^2} = \frac{3\gamma t}{2\eta r} \quad 7)$$

where x is the radius of neck growth between the spherical particles of radius r , γ is the surface tension, η is the viscosity of fused ash, and t is the time. The $(x/r)^2$ ratio can be taken as a criterion of the degree of sintering, i.e. the strength of boiler deposit (s) developed in time t , that is:

$$s = k \left(\frac{x}{r}\right)^2 \quad 8)$$

and the rate of deposit strength development is:

$$\frac{ds}{dt} = \frac{3k\gamma}{2\eta r} \quad 9)$$

where k is a constant.

Equation 9 shows that the rate of ash sintering, i.e. the development of cohesive strength of a deposit matrix is proportional to the surface tension and inversely proportional to the viscosity. The surface tension and particle size are not markedly changed by dissolution of sodium, iron or calcium oxides in the glassy phase of silicate ash. However, the viscosity is markedly changed by the oxides. In particular, an enrichment of sodium in the surface layer of the silicate ash particles can lead to a high rate of sintering.

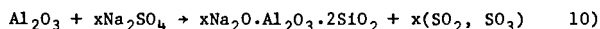
Some of the flame volatile sodium is dissolved in the vitrified silicate ash particles before deposition and an additional amount of sodium is transferred from the sulphate to silicate phases during sintering. The reaction between sodium sulphate and silicates at ash sintering temperatures has been monitored by thermo-gravimetric measurements. Some of the results are given in Table 4.

Table 4: Weight Loss of Sulphates and Sulphate/Silicate Mixtures

Sample	Na_2SO_4	$\frac{\text{Na}_2\text{SO}_4}{\text{KaOlin}}$	$\frac{\text{Na}_2\text{SO}_4}{\text{Ash}}$	CaSO_4	$\frac{\text{CaSO}_4}{\text{KaOlin}}$	$\frac{\text{CaSO}_4}{\text{Ash}}$
Loss Initiation Temperature, K	1425	1085	1175	>1525	1275	1275

Anhydrous sulphate samples and the sulphate/silicate mixtures (50 per cent by weight sulphate) were heated in air at the rate of 6 K per minute.

The results in Table 4 show that the reaction between sodium sulphate and kaolin commenced at 1085 K with the release of SO₂ and SO₃



A typical bituminous coal ash required a higher temperature of 1175 K for the sulphate decomposition reaction.

The transfer of sodium from the sulphate of silicate phase will reduce the viscosity of the glassy material resulting in an enhanced rate of sintering. At higher temperatures, above 1275 K, calcium sulphate starts to dissociate in the presence of kaolin and thus calcium oxide will be available for the sintering reactions. The specific roles of coal calcium and also the iron mineral species in ash sintering and slag formation have been discussed previously (2).

The sintering rates of bituminous, sub-bituminous and lignite coal ashes of different sodium contents can be determined by the electrical conductance measurements. In this method the conductance across an ash compact is measured and it is an indication of the degree of sintering (27). The sodium ions in the low viscosity glass and molten sulphate are the conductive species and the conductance continuity is provided by the sinter bridges between the particles.

Fig. 8 (curve B) shows that sub-bituminous coal ash of high (6.3 per cent) sodium oxide content commenced sintering at 1100 K as determined by the conductance measurements. The results (27) suggest that the amount of sodium in some ashes are sufficiently high both to initiate and sustain a rapid rate of sintering below 1200 K. In contrast, with low sodium coals the rate of ash sintering and the formation of boiler deposits are related to the calcium and iron contents of coal mineral matter. Several empirical formulae have been proposed for predicting the deposit forming propensity of the lignitic and bituminous coal type ashes based on the sodium content (28). These formulae indicate that a rapid build-up of boiler deposit is to be expected when sodium (Na₂O) content of bituminous coal exceeds 2.5 per cent, and that of lignite and sub-bituminous coal ashes is above 4 per cent.

The lignite type ashes have comparatively low fouling propensity when the sodium content is below 4 per cent because of the limited amount of clay minerals available for sintering reaction. That is, in some lignite and sub-bituminous coals there is an excess of sodium and calcium available for the high temperature reactions, and the rate of deposit formation depends on the silicate content of ash (2,9,30). The bituminous coal type ash has an excess of silicates, i.e. the ash is pyrochemically acidic and the rate of sintering depends on the availability of sodium, calcium and iron species in the flame heated deposit material.

The formation of sintered ash deposits is governed chiefly by viscous flow, and the rate of sintering (S_r) can be expressed in terms of the ratio of glassy material to crystalline species of silicate ash (R_{g/c}) and the viscosity of the glassy phase (η):

$$S_r = \kappa_1 (R_{g/c}) \frac{1}{\eta} \quad (11)$$

where κ is a constant. The characteristics of flame heated silicate particles, (Fig. 4 and Table 3 in Sect. 4) suggest that the vitrified potassium aluminosilicate particles and the below 5 μm diameter kaolinite particles are first to sinter after deposits. The particles will have a high glass content and the small size enhances sintering as evident from equation (10). It is therefore to be expected that the presence of floor material (6) should enhance sintering and

large particle quartz particles would retard the deposit formation. This applies in the absence of large concentrations of the flame volatile sodium, and non-silicate calcium and iron compounds. The flux material oxides will both increase the ash glass content and reduce the viscosity for sintering, Equation 11, and the composition of original silicate species is less important.

CONCLUSIONS

Silicate Minerals in Coal

The silicate minerals, kaolinite and potassium aluminosilicate species together with quartz constitute the bulk of mineral matter in most coals. The approximate amounts of different silicate species of the bituminous coal mineral matter can be estimated from ash analysis.

Flame Volatile and Silicate Sodium in Coal

Sodium is rapidly volatilized in the flame when it occurs in a non-silicate compound form, chiefly associated with chlorine in bituminous coals and combined with organic compounds in the lignite and sub-bituminous fuels. The fraction of sodium combined with coal silicates remains largely involatile in the pulverized fuel flame.

Flame Vitrification and Spheridization of Silicate Particles

The aluminosilicate particles vitrify and take a spherical shape in the flame and are partially recrystallized on cooling. Micro-needles of mullite up to 10 μm long and crystalloids of quartz are the principal devitrification products enveloped in a glassy material matrix. Large quartz particles originally present in coal are only surface vitrified and do not spheridize in the flame. The coalescence by sintering and fusion of the small aluminosilicate particles dispersed in the fuel substance occurs when the host coal particles burn in the flame. The products are sintered ash skeletons, cenospheres and plerospheres up to 250 μm in diameter.

Sodium Transfer to Silicate and Sulphate Phases

The flame volatile sodium is partly dissolved in the surface layer of vitrified silicate ash particles and partly sulphated. The sulphate particles, 0.1 to 2 μm in diameter can form on the surface of ash particles or in the flue gas via vapour phase reactions followed by sublimation on cooling. Some potassium sulphate is also formed from a fraction of the alkali-metal released on vitrification of potassium aluminosilicates in the flame.

Initial Stage in Ash Sintering

The sulphate phase can initiate ash sintering by bringing the silicate particles to close contact as a result of the surface tension force. Subsequent sintering proceeds by viscous flow and the rate of sinter bond growth is proportional to the surface tension of silicate glassy phase and inversely proportional to the particle size and the viscosity. The latter changes exponentially with temperature and thus the viscosity of silicate ash particles governs the rate of sintering at different temperatures.

Decomposition of Sulphate on Silicate Ash Sintering

Sodium sulphates in the initial material deposited on boiler tubes will be decomposed by the pyrochemically acidic silicates in ash when the deposit temperature exceeds 1085 K. The transfer of sodium from the sulphate to silicate

phase reduces the viscosity of the glassy material of silicate ash thus increasing the rate of sintering.

Sintering of High Sodium Coal Ashes

Some lignite and sub-bituminous coal ash contain sufficiently high quantities of the flame volatile sodium to initiate and subsequently to sustain a high rate of ash sintering leading to a rapid build-up of boiler deposit. With most bituminous coal ashes the volatile sodium plays a role in initiating sintering but the subsequent deposit and slag formation depends largely on the presence of calcium and iron flux oxides. In general terms, the rate of ash sintering is governed by the ratio of glassy material to crystalline species and the viscosity of the glassy phase.

ACKNOWLEDGEMENT

The work was carried out at the Central Electricity Research Laboratories and the paper is published by permission of the Central Electricity Generating Board.

LITERATURE CITED

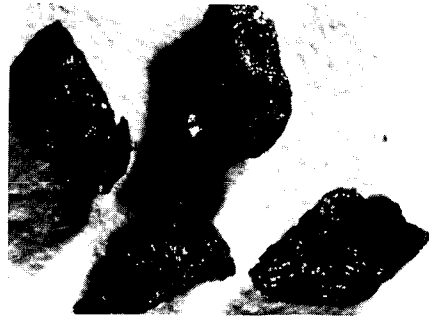
1. Raask, E., "Flame Imprinted Characteristics of Ash Relevant to Boiler Slagging, Corrosion and Erosion", Jour. Eng. Power (1982), 104, 858.
2. Raask E., "Mineral Impurities in Coal Combustion - The Behaviour, Problems and Remedial Measures", Hemisphere Publishing Corp., New York (1984).
3. Gumz, W., Kirsch, H. and MacKowsky, M-T., "Slagging Studies: Investigations of Minerals in Fuel and Their Role in Boiler Operation", Springer-Verlag, Berlin (1958).
4. O'Gorman, J.V. and Walker, P.L. "Mineral Matter and Trace Elements in US Coals", Dept. Interior Office of Coal Res. and Dev. Report No. 61, Washington, USA (1972).
5. Rao, C.P. and Gluskoter, J.H., "Occurrence and Distribution of Minerals in Illinois Coals", III. State Geol. Survey, Circular No. 476, Urbana, USA (1973).
6. Dixon, K., Skipsey, E. and Watts, J.T., "The Distribution and Composition of Inorganic Matter in British Coals: Part 2 - Alumino-Silicate Minerals in the Coal Seams of the East Midlands Coalfields", Jour Inst. Fuel (1970), 43, 124.
7. BCURA, "The Chemical Composition and the Viscometric Properties of the Slags Formed from Ashes of British Coals", British Coal Utilization Research Association, Leatherhead, UK (1963).
8. Raask, E., "Sulphate Capture in Ash and Boiler Deposits in Relation to SO₂ Emission", Prog. Energy Combust. Sci., (1982), 8, 261.
9. Sondreal, E.A., Kube, W.R. and Elder, J.L., "Analysis of the Northern Great Province Lignites and Their Ash: A Study of Variability", US Bureau of Mines, Report No. 7158, Washington, USA (1968).
10. Kiss, L.T., "The Mode of Occurrence and Distribution of Inorganic Elements in Australian Brown Coal", Coal Science Conference, E7 p. 774, Dusseldorf, W. Germany (1981).

11. Francis, W., "Coal, its Formation and Deposition", Arnold, London (1961).
12. Daybell, G.N., "The Relationship between Sodium and Chlorine in Some British Coals", Jour. Inst. Fuel (1967), 40, 3.
13. Skipsey, E., "Relationship between Chlorine in coal and the Salinity of Strata Waters", Fuel (1975) 54, 121.
14. Dunham, K.C., "Mineralization by Deep Formation Waters: A Review", Trans. Inst. Min. Metal, (1970), 79, B127.
15. Frenkel, J.S., "Viscous flow at Crystalline Bodies under the Action of Surface Tension", Jour. Phys. (Moscow) (1945), 9, 385.
16. Raask, E., Slag-Coal Interface Phenomena, ASME Jour Eng. Power (1966), Jan. p. 40.
17. Raask, E., "Fusion of Silicate Particles in Coal Flames", Fuel (1969), 48, 366.
18. Raask, E. and Goetz, L., "Characterization of Captured Ash, Chimney Stack Solids and Trace Elements", Jour. Inst. Energy, (1981), 54, 163.
19. Raask, E. and Bhaskar, M.C., "Pozzolanic Activity of Pulverized Fuel Ash", Concrete Res., (1975), 5, 363.
20. Raask, E., "Surface Properties of Pulverized Coal Ash and Chimney Solids", (1981), 1, 233.
21. Raask, E., "Quartz, Sulphates and Trace Elements in PF Ash", Jour. Inst. Energy, (1980), 53, 70.
22. Raask, E., "Cenospheres in Pulverized Fuel Ash", Jour. Inst. Fuel (1968), 43, 339.
23. Halstead, W.D. and Raask, E., "The Behaviour of Sulphur and Chlorine Compounds in Pulverized Coal Fired Boilers", Jour. Inst. Fuel (1969), 42, 344.
24. Raask, E., "The Behaviour of Potassium Silicates in Pulverized Coal Firing", VGB Mitteilungen (Essen Germany) (1968) 48, 348.
25. Stinespring, C.D. and Stewart, G.W., "Surface Enrichment of Alumino-Silicate Minerals and Coal Combustion Ash Particles", Atm. Envir. (1981), 15, 307.
26. Adams, A.M. and Raask, E., "Complete Sulphates in Coal Fired Boiler Plant", Conf. Mechanism of Corrosion by Fuel Impurities, p. 196, Marchwood U.K., Butterworths Publ., London (1963).
27. Raask, E., "Sintering Characteristics of Coal Ashes by Simultaneous Dilatometry and Electrical Conductance Measurements", Jour. Therm. Anal. (1979), 16, 91.
28. Winegartner, E.C., "Coal Fouling and Slagging Parameters", ASME Research Committee Publication on Corrosion and Deposits from Combustion Gases, New York (1974).

29. Tufte, P.H., Gronhovd, G.H., Sondreal, E.H. and Selle, S.J., "Ash Fouling Potentials of Western Sub-Bituminous Coal as Determined in a Pilot Plant Test Furnace", Am. Power Conf., Chicago, USA (1976).
30. Sondreal, E.A., Gronhovd, G.H., Tufte, P.H. and Beckering, W., "Ash Fouling Studies of Low Rank Western US Coals", Conf. Ash Deposition and Corrosion due to Impurities in Combustion Gases, p. 85, Edited by R.W. Bryers, Hemisphere Publishing Corp. Washington (1978).



(a) ADVENTITIOUS



(b) INHERENT-WHITE PARTICLES

FIG. 1 MINERAL MATTER IN COAL

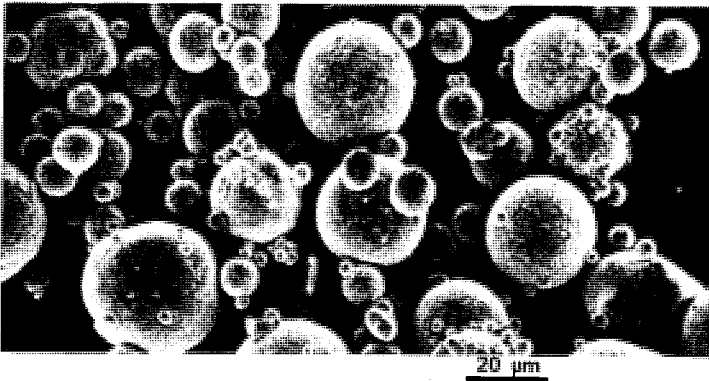
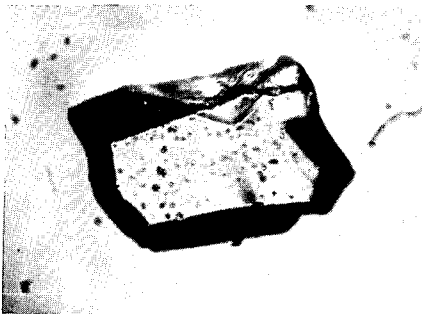
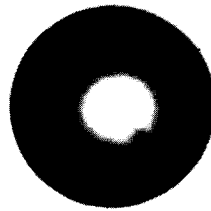


FIG. 2 PULVERIZED COAL ASH



(a)



(b)

FIG. 3 SURFACE FUSED (a) AND SPHERIDIZED (b) SILICATE PARTICLES

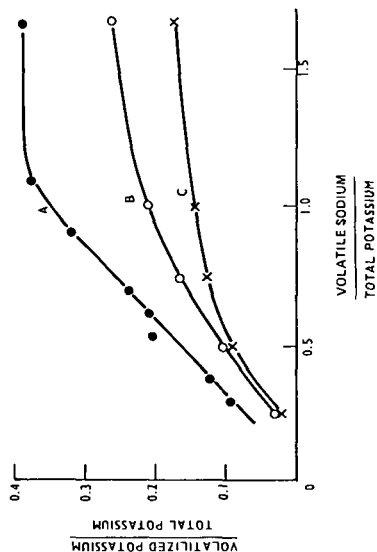


FIG. 4 THE EFFECT OF SODIUM CHLORIDE ON RELEASE OF POTASSIUM FROM SILICATES

- A - COAL SILICATES
- B - MUSCOVITE
- C - ORTHOCLASE

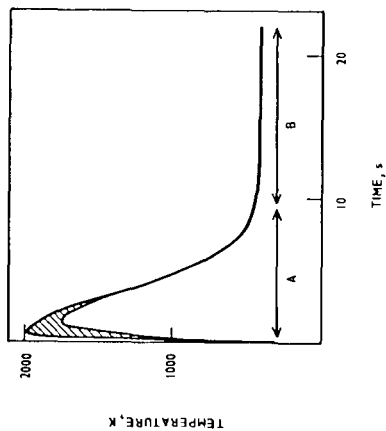
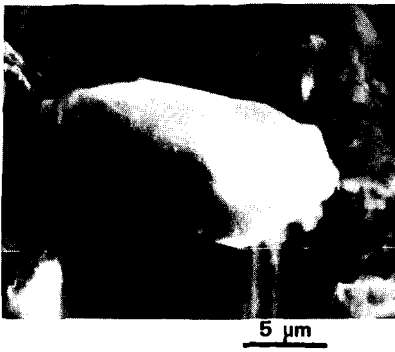
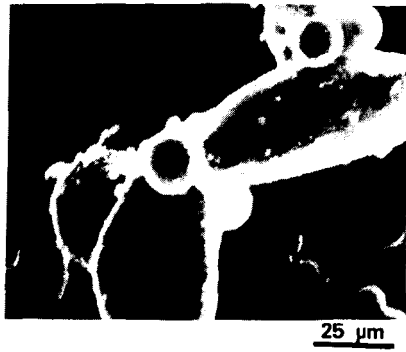


FIG. 5 TEMPERATURE/TIME PLOT FOR ASH PARTICLES IN A 500 MW PULVERIZED COAL FIRED BOILER - 0.1 μ m (TOP CURVE) TO 100 μ m (LOWER CURVE) SIZES

- SECTION A - COMBUSTION AND HEAT EXCHANGE CHAMBERS
- SECTION B - ELECTRICAL PRECIPITATORS AND CHIMNEY



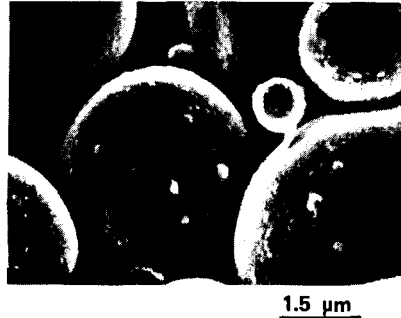
(a) UNFUSED QUARTZ PARTICLE



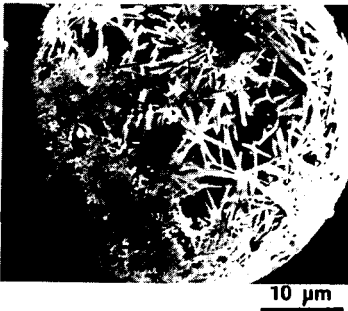
(b) ELONGATED SILICATE PARTICLES



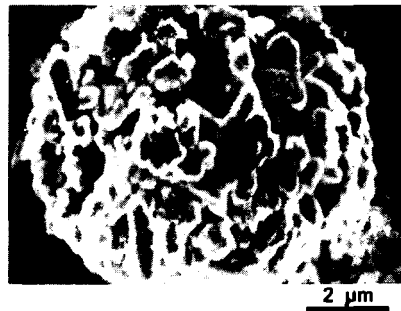
(c) MICROIDS ON ASH



(d) ACID CLEANED ASH

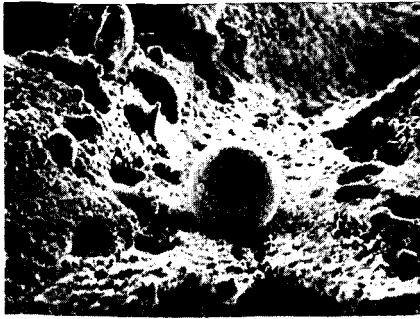


(e) MULLITE NEEDLES IN ASH

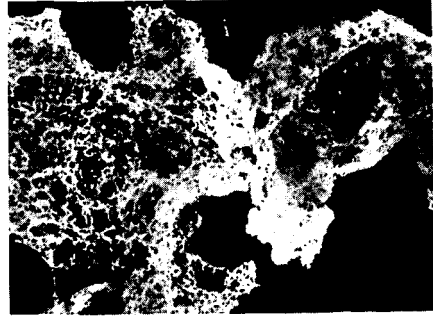


(f) QUARTZ CRYSTALLOIDS

FIG. 6 DIAGNOSTIC FEATURES OF FLAME HEATED ASH



10 μ m



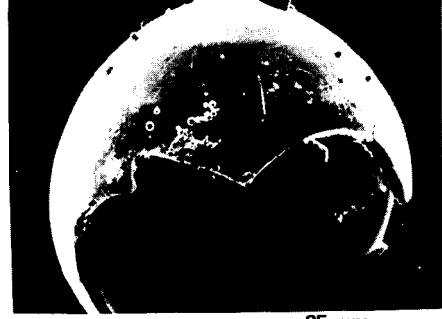
20 μ m

(a) ASH PARTICLES ON COKE

(b) ASH SKELETON IN COKE



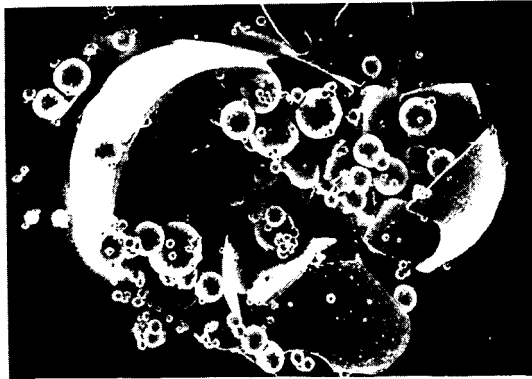
25 μ m



25 μ m

(c) CENOSPHERES

(d) FRACTURED CENOSPHERE



(e) PLEROSPHERE

25 μ m

FIG. 7 COALESCENCE PRODUCTS OF INHERENT ASH IN FLAME

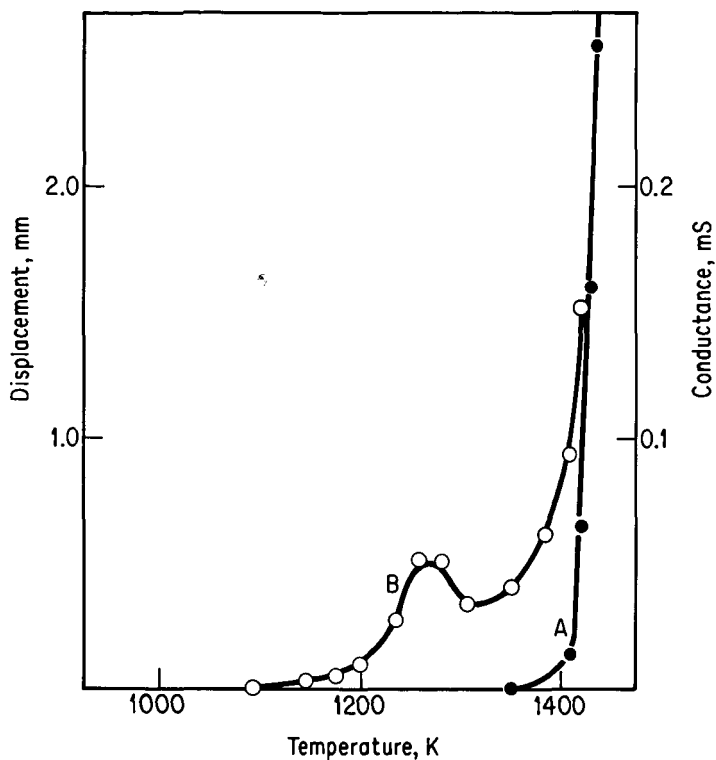


**FIG.8 SIMULTANEOUS SHRINKAGE AND CONDUCTANCE MEASUREMENTS
LEIGH CREEK (AUSTRALIA) COAL ASH**

A - SHRINKAGE
B - CONDUCTANCE

VISCOSITY OF SYNTHETIC COAL ASH SLAGS

Karl S. Vorres and Sherman Greenberg†

Chemistry Division, Building 211
†Materials Science and Technology Division, Building 212
Argonne National Laboratory
9700 South Cass Avenue
Argonne, Illinois 60439

INTRODUCTION

Coal used for energy conversion contains a considerable amount of mineral matter. During the conversion process the mineral matter is heated, and in the higher temperature reactors is converted to a molten material which flows from the reactor at a rate dependent on the viscosity of the slag. In studies of coal slags obtained from electric utility boilers (1,2,3) this behavior has been studied and correlations have been determined between the viscosity of the slag and the chemical composition. These studies have been carried out in a range of gaseous environments typical of the combustion furnace with a range of oxygen concentrations from almost zero to 15%.

The purposes of this study included a determination of the viscosity behavior of synthetic slags over a range of compositions and temperatures characteristic of slagging gasifier operation. The compositions were chosen to be broadly representative of a range of coals from both the eastern and western U.S. The temperatures were chosen to be in the range of satisfactory gasifier operation, and within the limits of the experimental equipment. The gaseous environments were selected to have the low oxygen partial pressure (about 10^{-8} to 10^{-9} atm) typical of the slagging gasifier.

The viscosity data were to be used as input for an associated refractory/slag corrosion program. Accordingly, the data obtained for the first few slags were compared with correlations developed by Watt and Fereday (1,2) based on chemical composition and by Hoy, Roberts and Williams (3), using a modified version of the silica ratio. In order to simplify the systems for study, the synthetic slags were limited to the five components: SiO_2 , Al_2O_3 , FeO , CaO and MgO . Since they contained no Na_2O or K_2O , the slag compositions were outside the range of the earlier correlations. If this difference was neglected, then the composition of all but four of the synthetic slags used in this program fell outside the range of the compositions for which the correlations were developed (10% Al_2O_3 or 0% MgO or low silica ratio or high $\text{SiO}_2/\text{Al}_2\text{O}_3$ ratio) and the correlations did not, in general, represent the data obtained for the synthetic slags.

EXPERIMENTAL

Slag: The viscosities of 21 synthetic slags, covering the range of compositions expected in slags derived from American coals were determined in this

study. The synthetic slags were prepared from reagent grade chemicals. The synthetic slags were mixed with water and pressed into pellets using a pressure of 15000 psig. The pellets had a slightly smaller diameter than that of the containment crucible. The composition of the slags is given in Table 1.

Viscometer: The apparatus and technique have been described in detail (4). Essentially a Brookfield Rheolog(TM) was used to replace the sample head in the rotating cylinder slag corrosion apparatus used in slag/refractory corrosion studies at ANL (5). Appropriate seals and ceramic structural components permit maintenance of the desired low oxygen activity within the measuring chamber. The viscosity measuring "bob" was a cylinder 12.7 mm diameter and 11.1 mm high. For measurement at lower oxygen partial pressures the "bob" and connecting shaft were fabricated of molybdenum; in an air environment the molybdenum was replaced by platinum. The slag was contained in Al2O3 crucibles. The "bob" and measuring system were calibrated at room temperature using a series of NBS oils ranging from 10 to 600 poise.

Procedure: Viscosity measurements were usually made in a decreasing temperature mode at 50 C. intervals after the slag sample had been slowly heated to the desired temperature, typically about 1400-1550 C. The slag was kept at each temperature long enough to demonstrate constant viscosity (about 30-60 minutes). In one case, slag 12, measurements were also made in an increasing temperature mode to determine if there were hysteresis effects. None were observed in this slag and other work confirmed this (4). Measurements made in other laboratories with other slags have shown hysteresis (6). The desired oxygen partial pressure was maintained by flowing H₂-CO₂-N₂ (or A) mixtures of the required composition through the interior of the measuring chamber throughout the experiment. The variation of oxygen partial pressure with gas composition and temperature was calculated using a NASA-developed code (4).

RESULTS AND DISCUSSION

The data obtained were plotted as viscosity versus temperature for the different materials and displayed the expected exponential increase in viscosity as the temperature decreased. In most of the runs a characteristic sudden increase in viscosity was noted, as in some related studies (1,3). Some typical results are shown and compared with the Watt-Fereday and modified silica ratio projections, assuming a liquid phase, in Figures 1 and 2, (slags 1 & 12).

To understand the Newtonian characteristics of the slags, plots of logarithm of viscosity versus temperature were made. These indicated straight lines or two line segments. For runs with a sudden increase in viscosity at lower temperatures, two segments were observed. Shear rates were not varied and the various types of non-Newtonian behavior were not explored. The observed straight lines are consistent with Newtonian behavior.

Arrhenius plots were then made. These plots typically involve the logarithm of a rate constant and the reciprocal of the absolute temperature. Viscosity is not a rate parameter, but is defined as the shear stress divided by the shear rate. The reciprocal of the viscosity is the shear rate per unit shear stress and was used in the plots. A typical example is shown in Figure 3. Slag 1 shows a typical high temperature low activation energy regime with a transition to a high activation energy, low temperature regime. This behavior was noted in most of the

runs. The other behavior was, as in the case of slag 12, a single straight line covering the range of the data. The slopes and activation energies for runs without the transition tended to be intermediate in the range of the values for runs with the transition.

In order to compare the viscosity behavior of the different compositions for the higher temperature regime and the slags with no transitions, separate plots superimposing the sample series with a constant weight % SiO₂ were made and are shown in Figures 4,5 and 6. Note the vertical change in scale in Figure 6. The solid portion of the lines represents the actual range of data. The dashed part of the lines was added to facilitate visual comparison. Examination of the plots shows two general tendencies. The reciprocal viscosities or fluidities tend to increase for series with lesser amounts of SiO₂ in them. Although the envelopes of data are broad, this observation can be made. Additionally, for a given series with a fixed weight % SiO₂, the fluidities are greater for the lower amounts of Al₂O₃.

A similar study of the lower temperature regime will be made later.

Activation energies and the temperature range of data are given in Table 2. Initial statistical analyses have not shown a strong correlation of activation energies with any of the slag constituents.

A wide range of activation energies with very high values was obtained for the lower temperature regime. The transition from the higher to the lower temperature regime generally occurred in the 1300-1400 C range. In order to interpret the data the ternary equilibrium phase diagrams for the systems SiO₂-Al₂O₃-MO were examined where MO is either CaO, FeO, or MgO. The mole fractions of each of the constituents were calculated as also shown in Table 2, and the ternary diagram corresponding to the major base in the group CaO, FeO or MgO was selected. Usually a ternary eutectic was found in the temperature region which would be expected for a system most closely corresponding to the sample composition. This eutectic temperature was close to the observed transition temperatures in the viscosity data. Many of the highest temperatures used were significantly below those associated with the appearance of a solid phase from the melt. This solid phase could have been present through the entire series of measurements on the slag.

CONCLUSIONS

A series of 21 synthetic coal ash slags were studied. It was observed that: (1) Plots of the logarithm of viscosity versus temperature showed one or two straight line segments, indicating Newtonian behavior in the temperature range studied. (2) Plots of the logarithm of the reciprocal of viscosity versus reciprocal of absolute temperature also showed one or two straight line segments, indicating one or two mechanisms were operative over the temperature range. (3) For three series, varying in SiO₂ content, those with the greatest SiO₂ content had the highest viscosities. (4) Within a series of given SiO₂ content, those members with the highest Al₂O₃ content had the highest viscosity. (5) For slags exhibiting a transition in behavior, the transition temperature could usually be associated with a ternary eutectic temperature in the phase equilibrium diagram for the most closely related ternary system. (6) Many of the slags probably had a

solid phase precipitating from the liquid phase during the cooling period before the transition temperature.

ACKNOWLEDGMENTS

The authors gratefully acknowledge the support of the U. S. Department of Energy. KSV acknowledges support from the Chemical Sciences Division of the Office of Basic Energy Sciences, while SG acknowledges support from the Surface Gasification Materials Program.

REFERENCES

1. J. D. Watt and F. Fereday, "The Flow Properties of the Slags Formed from the Ashes of British Coals. Part I. Viscosity of Homogeneous Liquid Slags in Relation to Slag Composition", J. Inst. Fuel 42, 101 (1969).
2. J. D. Watt, "The Flow Properties of Slags Formed from the Ashes of British Coals. Part 2. The Crystallizing Behavior of the Slags", J. Inst. Fuel 42, 131 (1969).
3. H. R. Hoy, A. G. Roberts, and D. M. Williams, "Behavior of Mineral Matter in Slagging Gasification Processes", IGE Journal 5, 444 (1965).
4. J. Chen, S. Greenberg, and R. Poeppel, "The Viscosity of Coal Slags as a Function of Composition, Temperature and Oxygen Partial Pressure", ANL/FE-83-30 (in press).
5. S. Greenberg, R. Poeppel et al, "The Corrosion of Ceramic Refractories in Synthetic Coal Slags Using the Rotating Cylinder Technique: An Interim Report", ANL/FE-83-31 (in press).
6. R. C. Streeter, E. K. Diehl and H. H. Schobert, "Measurement and Prediction of Low-Rank Coal Viscosity", Preprints Am. Chem. Soc. Div. Fuel Chem. 28(4) 174 (1983).

TABLE 1 SLAG COMPOSITIONS

COMPOSITION	NO.						
	1	2	3	4	5	6	7
SiO ₂	50	50	50	50	50	50	50
CaO	5	5	5	5	5	5	5
Al ₂ O ₃	10	10	20	20	20	30	30
FeO	15	25	25	15	5	15	5
MgO	20	10	0	10	20	0	10

COMPOSITION	NO.						
	8	9	10	11	12	13	14
SiO ₂	40	40	40	40	40	40	40
CaO	15	15	15	15	15	15	15
Al ₂ O ₃	10	10	20	20	20	30	30
FeO	15	25	25	15	5	15	5
MgO	20	10	0	10	20	0	10

COMPOSITION	NO.						
	15	16	17	18	19	20	21
SiO ₂	30	30	30	30	30	30	30
CaO	25	25	25	25	25	25	25
Al ₂ O ₃	10	10	20	20	20	30	30
FeO	15	25	25	15	5	15	5
MgO	20	10	0	10	20	0	10

Table 2. Activation Energies, Range of Temperatures and Mole Fractions

Slag #	Ea	Temperature Range	Mole Fractions				
			SiO ₂	Al ₂ O ₃	CaO	FeO	MgO
1	43.9	1440-1332	.483	.057	.052	.121	.288
2	44.2	1460-1314	.515	.061	.055	.215	.154
3	42.0	1456-1350	.568	.134	.061	.237	.000
4	40.1	1513-1337	.529	.125	.057	.133	.158
5	60.2	1462-1312	.495	.117	.053	.041	.295
6	366	1550-1500	.584	.209	.063	.147	.000
7	65.2	1515-1415	.543	.192	.058	.045	.162
8	77.6	1353-1192	.384	.056	.154	.120	.286
9	13.1	1455-1297	.409	.060	.164	.214	.152
10	55.5	1454-1335	.451	.133	.181	.235	.000
11	37.6	1439-1310	.420	.124	.169	.132	.156
12	103	1436-1262	.393	.116	.158	.041	.293
13	36.9	1535-1447	.464	.205	.186	.145	.000
14	50.8	1484-1401	.431	.190	.173	.045	.161
15	104	1434-1339	.286	.056	.255	.119	.284
16	77.6	1390-1265	.272	.060	.272	.212	.151
17	29.5	1451-1299	.335	.132	.299	.234	.000
18	106	1448-1377	.313	.123	.279	.131	.155
19	20.0	1459-1352	.293	.115	.261	.041	.291
20	55.1	1402-1294	.345	.203	.308	.144	.000
21	116	1532-1415	.321	.189	.286	.045	.159

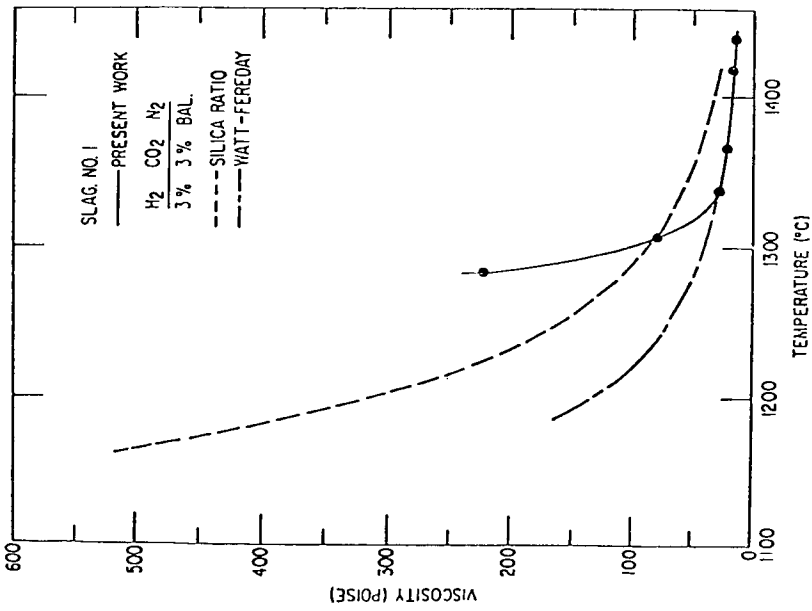


Figure 1. Viscosity of Slag 1

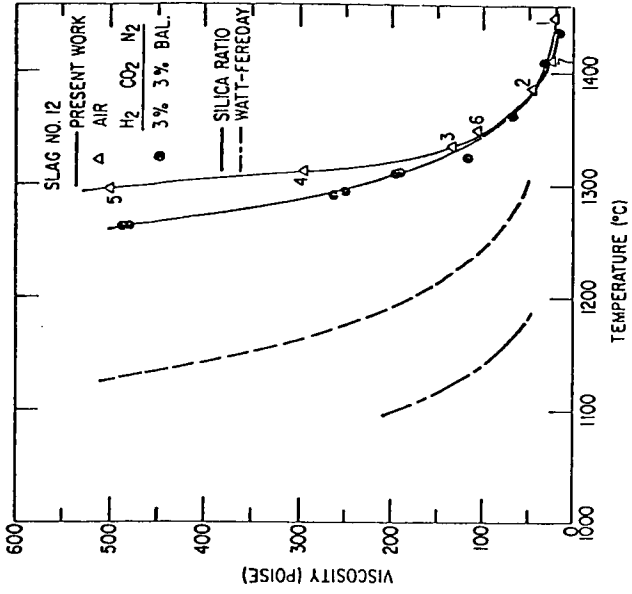


Figure 2. Viscosity of Slag 12

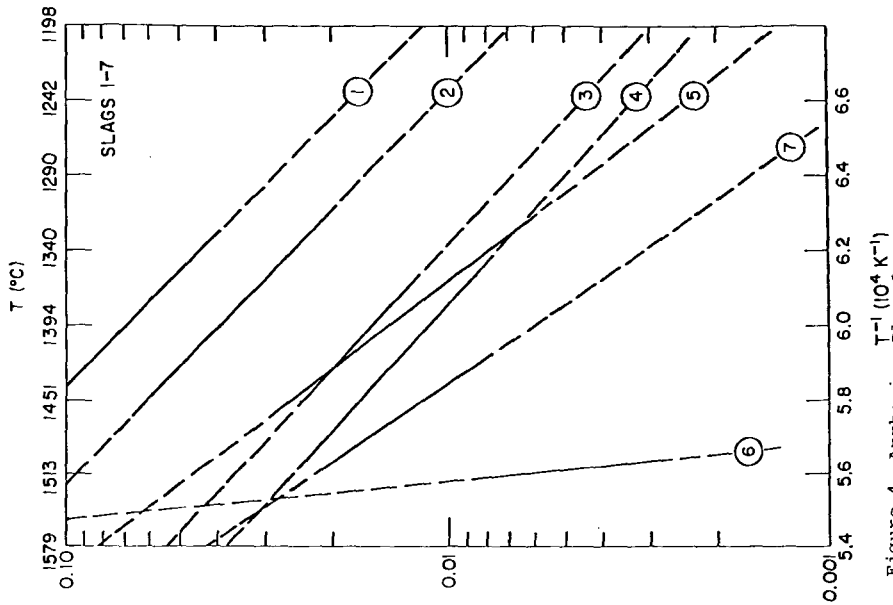


Figure 4. Arrhenius Plot for Slags 1-7

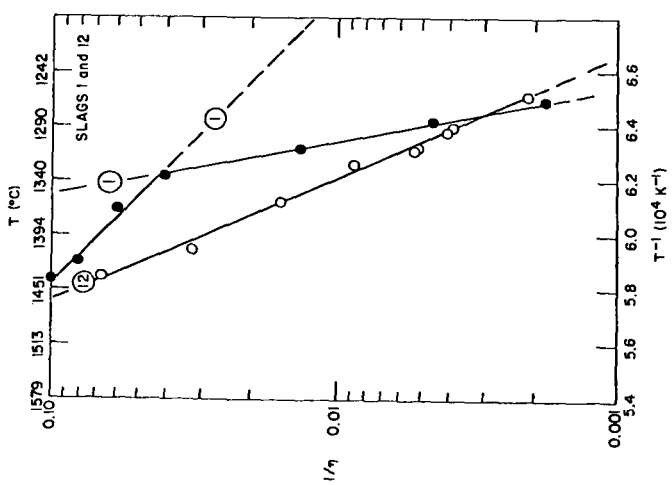
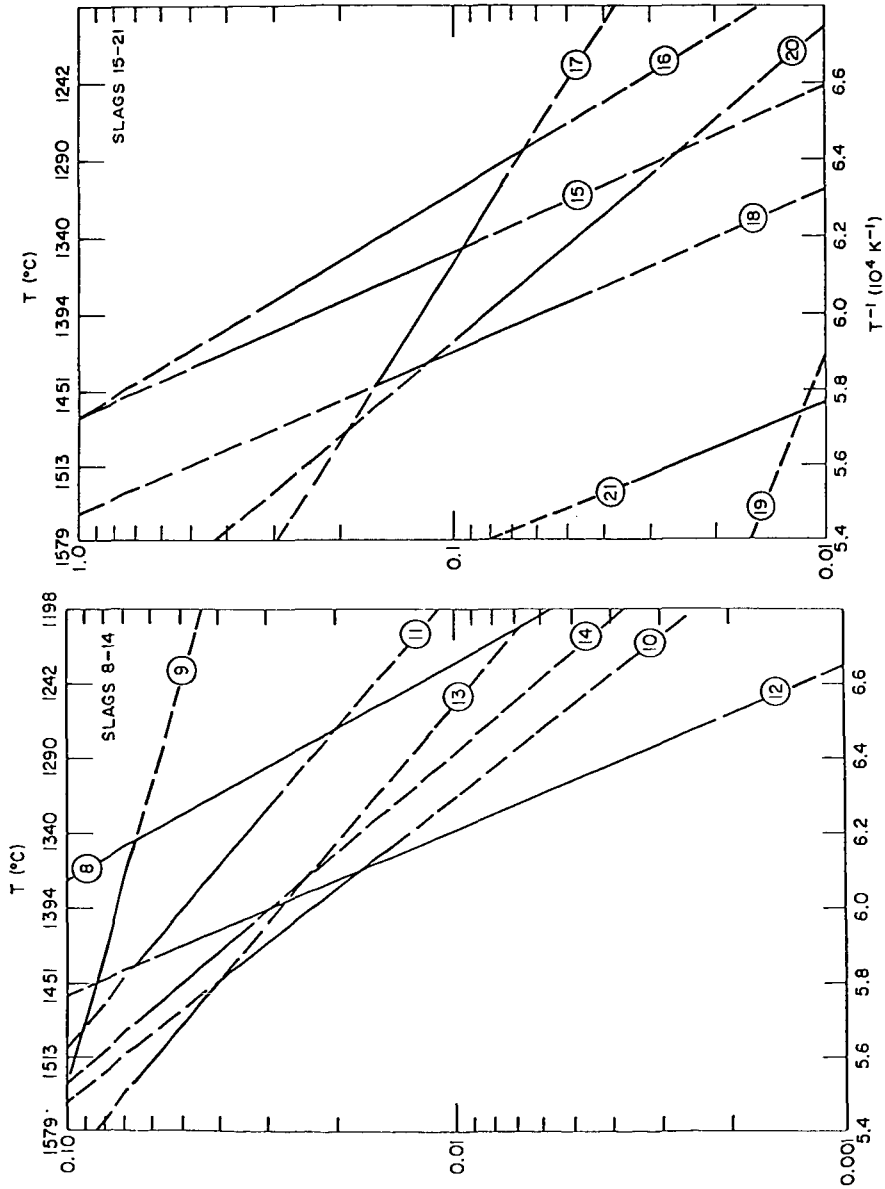


Figure 3. Typical Arrhenius Plots



Arrhenius Plots of Logarithm of Reciprocal Viscosity and Reciprocal Absolute Temperatures for Slags 8-14 and 15-21

SULFUR SOLUBILITY IN SLAGS FOR CYCLONE COAL COMBUSTORS

by

David H. DeYoung

Smelting Process Development Division
Alcoa Laboratories
New Kensington, PA 15068

I. INTRODUCTION

This study was conducted to select potential slag compositions for use in a slagging, staged, cyclone coal combustor, and to obtain the necessary data to evaluate the desulfurizing ability of the combustor. The first stage of such a combustor would be operated quite reducing to facilitate sulfur removal by a slag formed from the coal ash and inorganic additives (e.g., lime). A tangential motion imparted to the gas would throw ash, coal, and additives to the combustor wall where they would combine to form a molten slag. This slag, containing some dissolved sulfur, would continually drain out of a taphole at the exit end of the horizontally-placed cylindrical combustor. Advantages of this type of combustor are removal of some sulfur, low particulate emissions, and low NO_x emissions.

This paper will be divided into three parts. First, the selection of slag compositions will be outlined. Second, sulfide capacity measurements of these slags will be discussed. Third, the desulfurizing potential of a slagging, cyclone combustor will be evaluated using these measurements.

II. SLAG COMPOSITION SELECTION

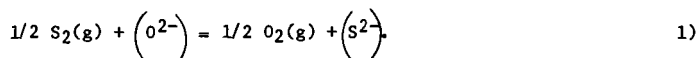
The strategy was first to select possible additives, then locate phase diagrams for systems of major ash components plus additives, and finally, select low-melting eutectic compositions as candidate slags. Additives were chosen for their known ability to form low-melting silicates (e.g., the alkalis) or for their known ability for desulfurization (e.g., the alkaline earth elements). An eastern coal was used for tests of a pilot combustor. Its ash composition, used to calculate additive compositions, is given in Table I. Major components, SiO_2 , Al_2O_3 , and Fe_2O_3 , account for approximately 80% of the ash.

Ternary phase diagrams for the SiO_2 - Al_2O_3 -additive and SiO_2 - FeO -additive systems were investigated for possible slag compositions. Unless otherwise noted, all phase diagrams were taken from Levin, et al (1-3) or Roth, et al (4). The selected compositions which were tested are given in Table II, as are estimated liquidus temperatures. Obviously, the liquidus temperature of the slag consisting of coal ash and the additive will be different from those given by the phase diagrams because of the minor components of the ash. However, the phase diagrams provide reasonable initial selections. Additive compositions and quantities are given in Table III.

III. SULFIDE CAPACITY MEASUREMENTS

Sulfide capacities of the selected slag compositions were measured to rate the slags and to provide data for evaluation of the operation of a combustor with these slags.

Chemistry of Sulfur in Slags: There has been considerable research on the chemistry of sulfur in slags reported in the literature. Most was aimed toward understanding and improving the desulfurization of iron and steel. These studies (5-7) have shown that at high oxygen potentials sulfur dissolves in slags as a sulfate, and at low oxygen potentials, the condition relevant to the two-stage combustor, sulfur dissolves as a sulfide. This can be represented by the reaction,



A quantity called the sulfide capacity (6) can be defined as:

$$C_S \equiv (\text{wt } \% S) \left(\frac{P_{O_2}}{P_{S_2}} \right)^{1/2} \quad 2)$$

where wt % S refers to sulfur dissolved in the slag, and P_{O_2} and P_{S_2} are the partial pressures of oxygen and sulfur in the atmosphere with which the slag is equilibrated. The sulfide capacity for many slags has been found (5,6) to be independent of sulfur and oxygen potentials for wide ranges, and therefore is a useful quantity for rating slags. One exception relevant to this study is that, for slags containing FeO, C_S is expected to change with oxygen potential as the ratio of ferrous to ferric ions in the slag changes.

A review of the literature (5-22) showed that virtually all work on sulfur in slags was on systems relevant to the desulfurization of iron and steel and at temperatures ranging from 1400-1600°C. No data were found for low-melting slags (liquidus temperatures, approximately 1000-1100°C), and particularly for the iron-alkali-aluminosilicates from which many of the proposed compositions are composed. Therefore, experimental measurements were necessary to obtain the data needed for selection of slags.

Experimental Method: An equilibration technique was chosen to measure the sulfide capacities of the candidate slags. Slag samples were equilibrated with a CO-CO₂-SO₂ gas mixture having fixed oxygen and sulfur potentials, quenched to room temperature, and analyzed for sulfur. Sulfide capacities were then calculated from the sulfur concentrations using Equation 2. This technique was chosen because it is a direct method, and because the oxygen and sulfur potentials could be accurately controlled, and, if necessary, these could be set to match the activities for oxygen and sulfur which were anticipated in the actual coal combustor. The apparatus used for sulfide capacity measurements is shown schematically in Figure 1.

Slags were prepared by mixing preweighed amounts of additives and coal ash. The coal ash was obtained from Bituminous Coal Research, Inc. It was prepared by ashing Loveridge Seam, West Virginia coal in air at 750°C, followed by a reduction in a 60%CO-40%CO₂ gas at 1000°C, then cooled under nitrogen.

The gas compositions for each experiment were chosen to obtain as low an oxygen potential as possible, without reducing FeO to Fe metal. They were also chosen to obtain as low a sulfur potential as possible to match anticipated conditions in the actual combustor, yet large enough so that they could be prepared by mixing gases. The equilibration time for slag samples was determined by periodic analyses of the gas exiting the reactor. Quenched slag samples were analyzed for sulfur using a Leco titrator, and were analyzed for Si, Al, Fe, Na, K, Ca, Mg, Ti, and P by atomic absorption.

Results: Table IV gives the results for all sulfide capacity measurements. Figures 2 and 3 show ternary phase diagrams for selected systems on which the results are shown. Compositions shown were obtained by taking the three major components from the slag analyses and normalizing to 100%. The sulfide capacities are shown as a function of basicity in Figure 4, which summarizes all results of this study. Molar basicities (Σ mole fraction bases/ Σ mole fraction acids) were calculated from the slag analyses.

It was found that after equilibration with the sulfurizing gas, certain slags in the $\text{FeO-Al}_2\text{O}_3\text{-SiO}_2$ system consisted of two immiscible liquids at 1100°C . One phase was a glass. The other phase had a metallic appearance and will be referred to as the "matte phase". The sulfide capacities for these slags should be considered as "apparent" because the sulfide capacity is defined for a single liquid phase. The matte phase in all of these double-phased slags contained 27-31% S, while the glass phase contained from 0.2 to 13% S. X-ray diffraction analyses showed the glass phase to be amorphous and the matte phase to contain FeS and FeS_2 .

Discussion: Slag compositions 2-A-1, 2-A-7, 2-B-2, 2-C-1, 2-D-2, and 2-E-1 were closest to the coal ash composition given in Table I, containing 25-38% additive. As seen from Table IV, $\log C_S$ ranged from approximately -3.8 to -5.5 at 1100°C . Using the basicity of the ash calculated from Table I and the data shown in Figure 4, the sulfide capacity for pure ash is estimated to be approximately $\log C_S = -5.2$. This is quite low as compared to results obtained for slags containing significant quantities of additives. As will be demonstrated later in the report, sulfur captured by coal ash slag with this sulfide capacity would be insignificant even at very favorable conditions - very low oxygen potential and low temperature.

There is a general correlation between sulfide capacity and basicity for a given system, as shown in Figure 4. There is a sharp drop in sulfide capacity between basicities of 1.0 to 0.5, which corresponds to the metasilicate to disilicate compositions in a binary silicate. For a given basicity, systems 2-A (FeO) and 2-C (FeO, CaO) have significantly higher sulfide capacities than systems 2-D (Na_2O) and 2-E (CaO), so that for a given basicity, FeO is superior to CaO and Na_2O as an additive. This is not what would be expected considering the standard free energies of formation of the sulfides and oxides of Fe, Ca, and Na.

Considering standard free energies for the formation of metal sulfides from metal oxides, FeO and CaO should be approximately equivalent desulfurizers and Na_2O should be superior. However, slags are far from ideal solutions because of the strong interactions among species -- particularly with SiO_2 . This is why experimental measurements of sulfide capacities were needed. Free energy of mixing data (24) for Na_2O , CaO, and FeO binary silicates show that the chemical interaction with silica decreases in the order Na_2O , CaO, FeO, and for a given basicity, the activity of the basic oxide in the silicates increase in the order Na_2O , CaO, and FeO. On this basis, FeO should be a better desulfurizer than CaO or Na_2O . This is consistent with the present results. Not surprisingly, the metal oxide-silica interaction is a major factor in the desulfurization ability of the slag.

Several modifications of slags based on the $\text{FeO-Al}_2\text{O}_3\text{-SiO}_2$ system were tested to determine if a less expensive additive could be substituted for some of the iron or if additives could be used to reduce liquidus temperatures. Figure 4 shows that replacing a portion of the iron oxide in slags of the $\text{FeO-Al}_2\text{O}_3\text{-SiO}_2$ system with CaO (5 wt %) or MgO (12 wt %) had no effect on the sulfide capacities. Results for composition 2-C-1 also support this conclusion, because for this composition approximately 14% of the FeO of an equivalent composition in the $\text{FeO-Al}_2\text{O}_3\text{-SiO}_2$ system was replaced by CaO, with only a slight decrease in sulfide capacity. Replacement of portions of the SiO_2 in $\text{FeO-Al}_2\text{O}_3\text{-SiO}_2$ slags by B_2O_3 or P_2O_5 has no effect on sulfide capacities; therefore, these additives are potentially useful for reducing slag liquidus temperatures.

Figure 5 compares some results of this study to those found in the literature for similar slags at higher temperatures. These literature data were adjusted to a basicity of 1.65 using data given in Figure 4. The data from this study are quite consistent with the literature data. The linearity of the sulfide capacity with inverse temperature is consistent with the theoretical relationship,

$$\frac{d \ln C_S}{d (1/T)} = -\Delta H^\circ/R + H_{FeO}^M/R - H_{FeS}^M/R \quad 3)$$

where ΔH° is the standard enthalpy change for the reaction,



and H_{FeO}^M and H_{FeS}^M

are the partial molar enthalpies of mixing of FeO and FeS in the slag. This relationship can be derived from Equation 2, the equilibrium constant for Equation 4 and the Gibbs-Helmholtz equation.

Most of the slags tested were found to have been partially or completely melted at 1100°C. However, at 1000°C, all slags from the FeO-Al₂O₃-SiO₂ system were not molten. It is thought that for these compositions the entire additive reacted with sulfur species in the atmosphere while none reacted with the SiO₂ or with other components in the ash. Hence, sulfide capacities measured from this experiment are not true sulfide capacities of the slags. Another point which supports this is that the "measured" sulfide capacities at 1000°C are greater than those at 1100°C, while Figure 5 shows the opposite trend for results for molten slags. Also, other literature data show that sulfide capacities generally increase with temperature.

This points out an inherent disadvantage in using a coal ash slag for desulfurization. When silica reacts with the desulfurizing agent, e.g., lime, the effectiveness of the desulfurizing compound is greatly reduced. Hence, it is desirable to design a desulfurizing combustor in which the ash does not react with the desulfurizing material.

IV. EVALUATION OF A PILOT COMBUSTOR

Calculations: The measured sulfide capacities were used to estimate sulfur emissions from a staged, slagging, cyclone combustor operating close to equilibrium. To calculate sulfur emissions, an equation for gas-slag chemical equilibrium for sulfur (Equation 2) and a mass balance for sulfur are solved simultaneously. First, the equilibrium gas compositions were calculated for the combustion of coal with air for a range of sulfur concentrations in the coal. This was done using Alcoa's Chemical Equilibrium Computer Program (23). Next, the concentrations of sulfur in the slags for equilibrium with the combustion gases were calculated. Finally, the quantity of additives needed to obtain these compositions were calculated from sulfur mass balances.

Results: Figure 6 shows an example of the results for these calculations, for combustion with 55% of stoichiometric air (stage 1) at 1100°C. A reasonable goal for the sulfur capture, considering projections of future EPA regulations, is 70%. The slag mass can vary between 85 and 350 g/kg coal (the upper limit was

established from a heat balance for Alcoa's pilot combustor), so the necessary $\log C_S$ for a 70% sulfur removal is between -2.75 and -3.3. A sulfide capacity of $\log C_S = -3.3$ at 1100°C was obtained for certain slags based on the FeO-Al₂O₃-SiO₂ system, e.g., compositions 2-A-3 or 2-A-10.

As the combustion stoichiometry is decreased, the curves in Figures 6 are rotated counterclockwise about the origin, i.e., the sulfur removal is increased. An increase in temperature will have the opposite effect. The curves are rotated clockwise about the origin. However, for a particular slag composition the sulfide capacity increases with temperature, as shown in Figure 5. The net result of the two opposing effects (using the temperature behavior shown in Figure 5) is that the sulfur removal decreases with increasing temperature. In the range of coal-sulfur contents investigated, 2-6%, the fraction of sulfur removed by slag does not change with sulfur content in the coal. The total sulfur emitted increases with increasing sulfur concentration in the coal, but the sulfur removal by the slag also increases.

A final point to note regarding sulfur removal is that as the concentration of hydrogen in the combustion gases is decreased, the sulfur removal by the slag will increase. This is due to the high stability of the hydrogen-sulfur species, such as H₂S(g), as compared to the carbon-sulfur species, such as COS. Thus, drying and charring of coal would significantly increase the theoretical removal of sulfur by the slag.

These calculations assume gas-slag equilibrium with respect to sulfur. This is probably only approached at the gas-slag surface near the exit of the first stage. At the entrance end of the combustor, the conditions would probably be more oxidizing than conditions calculated from the overall combustion stoichiometry, ϕ , and thus sulfur solubility in the slag would be less than that calculated. At some depth below the slag surface near this entrance end of the first stage, the conditions would be more reducing than those calculated from the overall combustion stoichiometry. This would result in increased sulfur solubility. The actual combustion process and sulfur removal processes are quite complex, and the extent of sulfur removal will depend on the combustion kinetics. For example, consider two extreme situations. In one, where most coal is combusted after it hits the slagged wall, sulfur removal should be relatively good. In the other extreme, where all the coal is combusted before it reaches the slagged wall, sulfur removal would be relatively poor because it would be dependent on mass transport through the gas phase, and the gas has a relatively short residence time.

In summary, the kinetics of the combustion process is important with regard to sulfur removal. The kinetics must be considered either by modelling or experimentation before a final judgment on desulfurization in a slagging, cyclone combustor can be made. The results of this study show that it is theoretically possible.

V. CONCLUSIONS

Sulfide capacity measurements of relatively low melting (approximately 1100°C in most cases) slags based on the FeO-Al₂O₃-SiO₂, FeO-Na₂O-SiO₂, FeO-CaO-SiO₂, Na₂O-Al₂O₃-SiO₂, and CaO-Al₂O₃-SiO₂ systems but composed of coal ash + additives, have shown that the FeO-Al₂O₃-SiO₂-based slags had the highest sulfide capacities. For a given basicity, the sulfide capacities could be ranked in the following order: FeO-Al₂O₃-SiO₂ > FeO-CaO-SiO₂ > FeO-Na₂O-SiO₂ > CaO-Al₂O₃-SiO₂ > Na₂O-Al₂O₃-SiO₂. The chemical interaction of the basic oxides with silica appears to be a dominant factor controlling the sulfide capacity. There was good correlation between sulfide capacity and slag basicity, and sulfide capacities increased with temperature.

Calculations of the equilibrium sulfur removal for a commercial combustor using the measured sulfide capacities, showed that it was theoretically possible to remove 70% or more of the sulfur in coal. The sulfur removal increases with decreasing temperature, decreasing combustion stoichiometry in the first stage of the burner, increasing slag flow, and decreasing content of hydrogen in the fuel. This work showed that a slagging, cyclone combustor can remove sulfur into the slag, but kinetic modelling and/or experimentation is needed to prove whether or not the concept will work.

VI. ACKNOWLEDGEMENT

This work was sponsored by the U.S. Department of Energy under Contract No. DE-AC07-78CS40037, "Pulverized Coal Firing of Aluminum Melting Furnaces."

VII. REFERENCES

1. E. M. Levin, C. R. Robbins, and H. F. McMurdie: Phase Diagrams for Ceramists, American Ceramic Society, Columbus, OH (1964).
2. E. M. Levin, C. R. Robbins, and H. F. McMurdie: Phase Diagrams for Ceramists, 1969 Supplement, American Ceramic Society, Columbus, OH (1969).
3. E. M. Levin and H. F. McMurdie: Phase Diagram for Ceramists, 1975 Supplement, American Ceramic Society, Columbus, OH (1975).
4. R. S. Roth, T. Negas, and L. P. Cook: Phase Diagrams for Ceramists, Volume IV, American Ceramic Society, Columbus, OH (1981).
5. G. R. St. Pierre and J. Chipman: Trans. AIME, v. 206, pp. 1474-1483 (1956).
6. C.J.B. Fincham and F. D. Richardson: Proc. R. Soc. Series A223, 40 (1954) and J. Iron Steel Ins. 178, 4 (1954).
7. F. D. Richardson: Physical Chemistry of Melts in Metallurgy, v. 2, pp. 291-304, Academic Press, London (1974).
8. P. T. Carter and T. G. McFarlane: J. Iron Steel Inst., 185, 54 (1957).
9. K. P. Abraham, M. W. Davies, and F. D. Richardson: J. Iron Steel Inst., v. 196, pp. 309-312 (1960).
10. K. P. Abraham and F. D. Richardson: J. Iron Steel Inst., v. 196, pp. 313-317 (1960).
11. E. W. Dewing and F. D. Richardson: J. Iron Steel Inst., v. 194, pp. 446-450 (1960).
12. R. A. Sharma and F. D. Richardson: J. Iron Steel Inst., v. 198, pp. 386-390 (1961).
13. R. A. Sharma and F. D. Richardson: J. Iron Steel Inst., v. 200, pp. 373-379 (1962).
14. G.J.W. Kor and F. D. Richardson: J. Iron Steel Inst. v. 206, pp. 700-704 (1968).
15. G.J.W. Kor and F. D. Richardson: Trans. AIME, v. 245, pp. 319-327 (1969).
16. R. J. Hawkins, S. G. Meherall, and M. W. Davis: J. Iron Steel Inst., v. 209, pp. 646-657 (1971).
17. A. Bronson and G. R. St. Pierre, Met. Trans. B, v. 10B, pp. 375-380 (1979).
18. A. Bronson and G.R. St. Pierre: Met. Trans. B, v. 12B, pp. 729-731 (1981).
19. H. B. Bell: Can. Met. Quart., v. 20 (2), pp. 169-179 (1981).
20. J. D. Shim and S. Ban-ya: Tetsu-to-Hagane, v. 68, pp. 251-60 (1982).
21. S. D. Brown, R. J. Roxburgh, I. Ghita, and H. B. Bell: Ironmaking and Steelmaking, v. 9, pp. 163-67 (1982).
22. I. Ghita and H. B. Bell: Ironmaking and Steelmaking, v. 9, pp. 239-43 (1982).
23. W. E. Wahnstedler: "Chemical Equilibrium Package Users Manual," Alcoa Laboratories Report No. 7-78-25.
24. D. R. Gaskell: Metallurgical Treatises, J. K. Tien and J. F. Elliott, ed., p. 60, TMS-AIME, Warrendale, PA (1981).

TABLE I. ASH FROM LOVERIDGE SEAM (WEST VIRGINIA) COAL

Component	Ash Analysis	
	Wt Pct.	Normalized (excluding sulfur and taking iron as FeO)
Al ₂ O ₃	18.4	24.1
SiO ₂	44.5	47.8
Fe ₂ O ₃	15.9	17.4 (FeO)
CaO	4.56	4.9
MgO	1.08	1.2
Na ₂ O	1.10	1.5
K ₂ O	1.11	1.3
TiO ₂	1.20	1.1
SO ₃	9.02	--
P ₂ O ₅	0.33	0.5

TABLE II. NORMALIZED COMPOSITIONS OF CANDIDATE SLAGS - MAJOR COMPONENTS ONLY

Slag No.	Composition, Wt. Pct.					Liquidus Temperature (°C) (Major Components Only)
	SiO ₂	Al ₂ O ₃	FeO	Na ₂ O	CaO	
2-A-1	46.0	19.9	34.1			1205
2-A-2	40.0	12.0	48.0			1083
2-A-3	18.1	5.9	76.0			1148
2-A-7	43.3	19.8	36.9			1220
2-A-8	35.3	14.1	50.6			1200
2-A-9	27.0	8.3	64.4			1150
2-A-10	23.6	5.9	70.4			1155
2-B-1	39.3		48.0	12.7		1000
2-B-2	56.4		21.8	21.8		?
2-B-3	33.2		26.2	40.6		1050
DSE-1	42.5		28.9	28.6		900
DSE-2	37.0		26.0	37.0		
2-C-1	37.7		46.4		15.7	1093
2-D-1	43.8	18.2		37.9		915
2-D-2	62.7	23.2		14.0		1063
2-D-3	61.6	12.2		26.2		732
2-E-1	42.1	20.1			37.8	1265
2-I-1	55.3	21.5	10.0	13.1		990

TABLE III. ADDITIVE COMPOSITIONS FOR CANDIDATE SLAGS

Slag No.	Additive Mass g/g Ash	Additive Composition, Wt. Pct.					
		SiO ₂	Al ₂ O ₃	Fe ₂ O ₃	Na ₂ CO ₃	CaO	Other
2-A-1	0.34	22.9		77.1			
2-A-2	1.20	27.0		73.0			
2-A-3	3.52	7.4		92.6			
2-A-4	3.74	7.0		87.2			5.8 % CaF ₂
2-A-5	3.52	1.6		92.6			5.8 % B ₂ O ₃
2-A-6	3.52	1.6		92.6			5.8 % P ₂ O ₅
2-A-7	0.36	13.9		86.1			
2-A-8	0.89	13.9		86.1			
2-A-9	2.19	13.9		86.1			
2-A-10	3.47	13.9		86.1			
2-A-10b	4.07	11.8		73.5			14.7 % MgO
2-A-11	3.49	7.5		86.7	2.5		3.4 % CaF ₂
2-A-12	4.99	13.9		86.1			
2-B-1	0.69			65.7	34.2		
2-B-2	0.30			3.9	96.1		
2-B-3	1.20			18.9	81.1		
DSE-1	0.69			24.2	75.8		
DSE-2	0.97			18.5	81.5		
2-C-1	0.61			75.5		24.5	
2-D-1	0.93	10.9			89.1		
2-D-2	0.40	43.8			56.2		
2-D-3	1.60	46.3			53.7		
2-E-1	0.43	6.3				93.7	
2-I-1	0.99	49.1	13.5		37.4		

TABLE IV. SULFIDE CAPACITY MEASUREMENTS

Exp't. No.	T (°C)	Run Time (h)	Slag Composition	Wt % S	Log C _S	Comments
2*	1100	24	DSE-1	4.22	-4.31	Did not melt
			"	5.34	-4.21	
			2-B-1	6.05	-4.16	
			2-B-2	0.26	-5.52	
			2-D-1	0.96	-4.96	
			2-D-2	0.87	-5.00	
4**	1100	115	DSE-1	4.31	-4.06	Sample crept out 2 phases 2 phases
			2-A-1	4.80	-4.01	
			2-A-2			
			2-A-3	22.5	-3.34	
			2-A-4	23.5	-3.32	
5**	1100	144.6	2-C-1	7.91	-3.79	2 phases 2 phases 2 phases 2 phases 2 phases Sample crept out
			2-A-5	20.2	-3.38	
			2-A-6	13.4	-3.56	
			2-A-7	5.06	-3.99	
			2-A-8	9.81	-3.70	
			2-A-9	16.6	-3.47	
			2-A-10	19.1	-3.41	
			2-A-11			
			2-B-3	2.65	-4.27	
			7***	1000	168.75	
2-A-4	25.1					
2-A-5	25.5					
2-A-6	24.1					
2-A-10	23.6					
2-A-11	24.2					
2-A-12	25.8					
2-A-3a	26.3					
2-I-1	0.44	-5.04				
11****	1300	70.0				2-A-3
			2-A-10	1.97	-3.00	
			2-A-10b	3.10	-2.80	

* Gas Composition - 70%CO-29.5% CO₂-0.5%SO₂

$$X_{O_2} = 7.2 \times 10^{-14}, X_{S_2} = 5.4 \times 10^{-4}$$

** Gas Composition - 70.2%CO-29.6%CO₂-0.25%SO₂

$$X_{O_2} = 6.8 \times 10^{-14}, X_{S_2} = 1.6 \times 10^{-4}$$

*** Gas Composition - 74.5%CO-25.3%CO₂-0.18%SO₂

$$X_{O_2} = 6.8 \times 10^{-14}, X_{S_2} = 1.6 \times 10^{-4}$$

**** Gas Composition - 66.3%CO-33.6%CO₂-0.14%SO₂

$$X_{O_2} = 4.9 \times 10^{-11}, X_{S_2} = 1.9 \times 10^{-4}$$

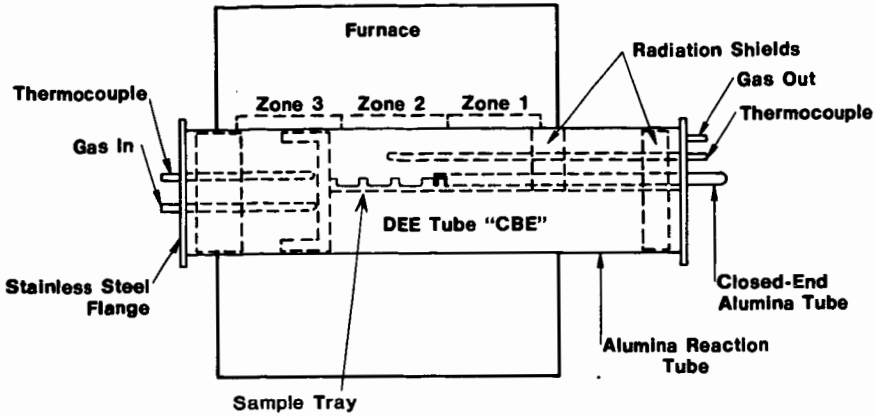


FIGURE 1. REACTOR USED FOR SULFIDE CAPACITY MEASUREMENTS.

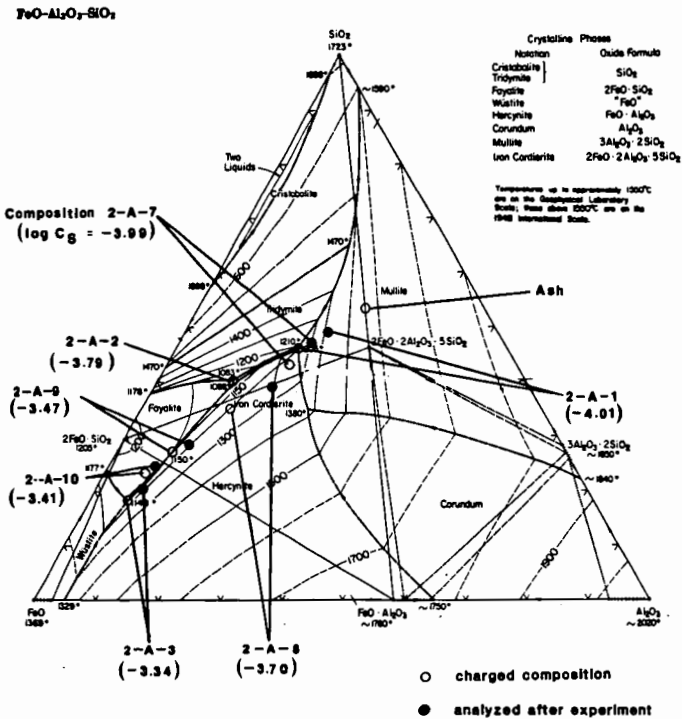


FIGURE 2. THE FeO-Al₂O₃-SiO₂ SYSTEM (2-A) WITH MEASURED SULFIDE CAPACITIES INDICATED. PHASE DIAGRAMS TAKEN FROM REFERENCE (1). OXIDE PHASES IN EQUILIBRIUM WITH METALLIC IRON.

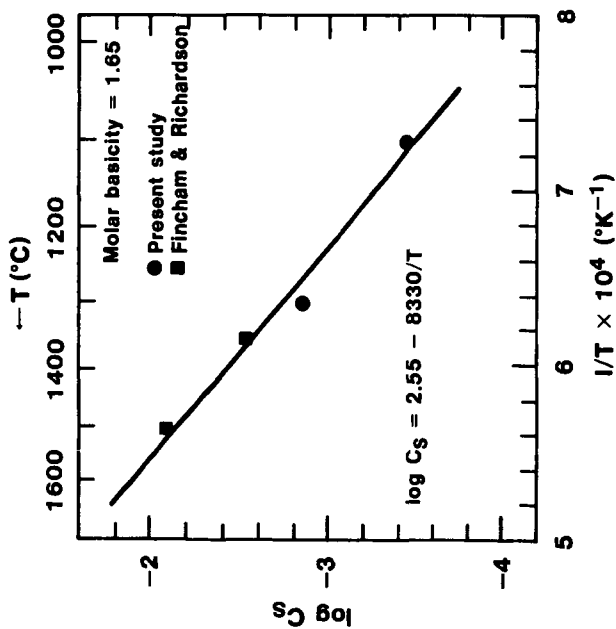


FIGURE 5. COMPARISON OF RESULTS FROM THIS STUDY TO THOSE OF FINCHAM AND RICHARDSON (6) FOR AN IRON SILICATE WITH MOLAR BASICITY OF 1.65. DATA FROM FINCHAM AND RICHARDSON WERE FOR PURE IRON SILICATES WHILE THESE FROM THE PRESENT STUDY CONTAINED SOME COAL ASH. DATA FROM FINCHAM AND RICHARDSON WERE CORRECTED FOR BASICITY USING DATA FROM THE PRESENT STUDY.

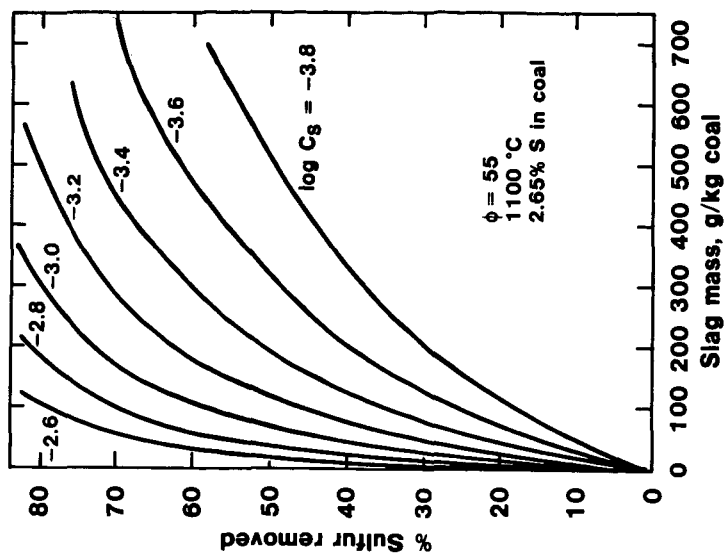


FIGURE 6. EQUILIBRIUM SULFUR REMOVAL BY SLAG FOR A COMBUSTOR OPERATING WITH LOVERIDGE SEAM (WEST VIRGINIA) COAL.

The Thermodynamic Properties of Molten Slags

Milton Blander* and Arthur D. Pelton†

INTRODUCTION

Silica based slag systems are highly ordered liquids which have been a difficult class of materials on which to perform thermodynamic analyses.¹⁻⁵ To our knowledge, no satisfactory, self-consistent prior method of analysis has been developed for systems as ordered and complex as silicates which incorporates all known data in a meaningful way. In this paper, we discuss the results of a method of analysis which permits one to simultaneously analyze a large amount of different types of data on binary systems. The calculations lead to a small set of parameters which permit one to calculate the thermodynamic properties of slag solutions as a function of temperature and composition. The thermodynamic self-consistency and the form of the equations used provide some confidence in the use of the results for interpolations and extrapolations outside the range of data. In addition, for systems in which silica is the only acid constituent, we propose a theoretically justified combining rule to calculate the properties of ternary systems based solely on data for the three subsidiary binaries. The results are in good agreement with available data.

The ionic nature of molten silicates suggests that many of the theories and correlations developed for molten salts⁶ can be applied to the development of correlations between the relative magnitudes of the deviations from ideal solution behavior in terms of ionic radii, charges, polarizabilities, dispersion interactions and ligand field effects.

CALCULATIONAL METHOD⁷

The molar free energy of mixing, ΔG_m of a silicate is represented by the expression

$$\Delta G_m = \sum_i RTX_i \ln X_i + \sum_i RTX_i \ln \gamma_i = \Delta G_m^{ideal} + \Delta G^E \quad (1)$$

where X_i is the mole fraction of component i , γ_i , the activity coefficient, represents deviations from ideal solution behavior of component i , ΔG_m^{ideal} is the molar free energy of mixing of a hypothetical ideal solution and ΔG^E is the molar excess free energy of mixing which represents the deviations from ideality of the molar free energy of solution. The conventional representation of $\ln \gamma_i$ and ΔG^E is a power series in mole fractions. The complexity of ordered solutions would require a very long power series in order to obtain a reasonable representation of their properties. This arises from the tendency of such solutions to have a "V" shaped dependence of the enthalpy of mixing and an "m" shaped dependence of the entropy of mixing on concentration.¹ The fitting of data using a long polynomial will generally be poor and ambiguous in such systems. In order to obtain reasonable fits, one must use equations which inherently have the concentration and temperature dependence of ordered solutions built in.

We have deduced a set of equations with such properties based on empirical modifications of the quasi-chemical theory. An energy parameter in the theory, W , is represented by a power series

*Argonne National Laboratory, Argonne, IL 60439

†Ecole Polytechnique, Université de Montréal, Montréal, Québec, Canada, H3C3A7

$$W = \sum_{j=0} C_j y^j \quad (2)$$

where y is an equivalent fraction of one of the components (silica is always chosen if present). For binary systems, the parameters C_j are deduced from a complex optimization procedure which performs a global and simultaneous analysis of all thermodynamic data on a system. This includes liquidus phase diagrams, activity data, data on miscibility gaps, enthalpies of fusion, free energies of formation of compounds, etc. The small set of resultant parameters (seven at most including temperature coefficients of some) are then used to recalculate the input data to double check the accuracy of the curve fitting procedure and the efficacy of the use of the equations for representing the data. The results were generally very good.

For multicomponent systems, we developed an asymmetric combining rule such that *e.g.* for a system 1-2-3 where 1 is silica, W_{12} and W_{13} which represent energies related to interactions of silica with the other two components, are a function only of y_1 , and W_{23} is related to the ratio $y_3/(y_2 + y_3)$. A partial theoretical justification for such a method can be based on theories for ternary systems.⁸

RESULTS OF THERMODYNAMIC ANALYSES

We have performed analyses of ten of the fifteen binary systems and six of the twenty ternary systems containing the components MgO, FeO, CaO, Na₂O, Al₂O₃, and SiO₂.^{7,9}

Table I
Systems Which Have Been Analyzed

Binary Systems		Ternary Systems
CaO-SiO ₂	CaO-AlO _{1.5}	CaO-AlO _{1.5} -SiO ₂
FeO-SiO ₂	NaO _{0.5} -AlO _{1.5}	NaO _{0.5} -CaO-SiO ₂
MgO-SiO ₂	MgO-FeO	NaO _{0.5} -AlO _{1.5} -SiO ₂
NaO _{0.5} -SiO ₂	MgO-CaO	CaO-FeO-SiO ₂
AlO _{0.5} -SiO ₂	CaO-FeO	CaO-MgO-SiO ₂
		MgO-FeO-SiO ₂

We illustrate our calculations for one ternary system below. The analysis of the three binary subsystems and the ternary system CaO-FeO-SiO₂ was performed using as input the liquidus phase diagram,¹⁰ activities of CaO,¹¹ and SiO₂,² the free energies of formation of CaSiO₃ and Ca₂SiO₄,¹³ and the miscibility gap¹⁴ in the CaO-SiO₂ system, measured activities of FeO in the CaO-FeO system,¹⁵ and the activities of FeO,^{16,17,18} the phase diagram¹⁹ and the free energy of formation of Fe₂SiO₄³ in the FeO-SiO₂ system. To illustrate some of the results, we exhibit (1) the calculated phase diagram of the FeO-SiO₂ system in Fig. 1 along with measured values of the invariant points and (2) a comparison of activities of "FeO" measured in the iron saturated molten FeO-SiO₂ system with calculated values in Fig. 2.

Using our "asymmetric" combining rules, the data for the binary systems were combined and led to the results for ternary systems given in Fig. 3; this figure illustrates the correspondence between calculated and measured values²⁰ of the activities of FeO in the CaO-FeO-SiO₂ system. The differences are well within the uncertainties in the measurements. We find that this method essentially permits us to make predictions in ternary systems based solely on data for the three

subsidiary binary systems for cases in which silica is the only acid component. When alumina and silica are both present, a more complex representation is necessary.

The good correspondence of calculations with the complex concentration dependence of activities in the CaO-FeO-SiO₂ system illustrates the fact that our equations properly take into account the kinds of ternary interaction terms known to exist in such systems.^{8,21} This feature lends confidence in the use of our equations for predictions in multicomponent systems (containing only silica as an acid component) based solely upon the subsidiary binaries. If, as it appears, this is generally true, our method provides an important predictive capability.

CORRELATIONS OF PROPERTIES

Theories and concepts which have been developed for molten salt solutions can be used to correlate the thermodynamic properties of silicates.⁶ Coulomb interactions lead to a dependence of thermodynamic functions on the inverse of the cation-anion interatomic distance. Thus, by analogy with molten salts, one would expect a linear dependence of the magnitudes of free energies of mixing on this parameter which is in a direction such that negative deviations from ideality increase in the order Li⁺, Na⁺, K⁺, Rb⁺, Cs⁺, and Mg⁺⁺, Ca⁺⁺, Sr⁺⁺, and Ba⁺⁺. In addition, monovalent alkali oxides should exhibit more negative deviations from ideality than divalent alkaline earth oxides. The polarizability of oxide anions leads to an additional contribution with a similar dependence on cations. The magnitude of cation-cation dispersion interactions are related to the polarizabilities, ionization potentials and interaction distances. Thus, the dissolution of oxides of cations with large dispersion interactions leads to a loss of this negative energy and hence to a positive contribution to deviations from ideality. In addition ligand field effects for divalent transition metals tend to contribute to negative deviations from ideal solution behavior in molten salts with monovalent cations. The effective charge of Si is greater than two and one would thus expect a positive contribution to deviations from ideal solution behavior from this source. The effect for Mn²⁺ which has a half filled shell for example, should be much less positive than for Fe²⁺.

The data for testing these influences on solution behavior are too sparse to reach quantitative conclusions. However, the general trends are in the right direction. Measured deviations from ideality of silicates with divalent oxides become more negative (or less positive) in the order Fe²⁺, Mn²⁺, Pb²⁺, Mg²⁺, Ca²⁺.^{1,7,9,22} In this view, ligand field effects lead to Fe²⁺ preceding Mn²⁺ and Mn²⁺ preceding even Mg²⁺ which has a smaller radius; dispersion interactions lead to Pb²⁺ preceding even Mg²⁺ even though its radius is larger than Ca²⁺ and Sr²⁺; finally, coulomb and polarization interactions lead to Mg²⁺ preceding Ca²⁺. With careful measurements of a larger number of binary silicate systems, it should be possible to develop useful correlations and a means of making reasonable predictions of the magnitudes of thermodynamic properties of silicates.

CONCLUSIONS

There are several significant conclusions which can be reached.

1. We have performed analyses of thermodynamic data on binary silicate systems which lead to a unique and accurate mathematical representation of their known properties.
2. Our use of equations which have the properties of ordered liquids built in appears to have the innate capability for representing a mass of different types of data on binary systems measured in various ranges of temperature and composition. This result lends confidence in the use of our analyses for interpolations and extrapolations outside the range of measurements.

3. We can theoretically justify an "asymmetric" combining rule which, for cases in which silica is the only acid component, leads to a *priori* predictions for ternary systems based on data for the three subsidiary binaries. It appears likely that such predictions would be valid for multicomponent systems.
4. A preliminary examination of thermodynamic data on silicates indicates that correlations developed for molten salts may be useful in understanding and ultimately in predicting magnitudes of the thermodynamic solution properties of silicates.

FIGURE CAPTIONS

1. Calculated phase diagram of the FeO-SiO₂ system. Numbers in parentheses are measured values from Muan and Osborne¹⁰ and Robie, et al.¹³
2. Activities of "FeO" measured in iron saturated molten FeO-SiO₂ at 1325°C (Δ)¹⁷, 1785°C (O)¹⁶, 1880°C (\diamond)¹⁶, and 1960°C (\square)¹⁶. The two solid lines represent calculated points at 1325°C and 1880°C. The filled circles along one solid line represent individual calculated points and the three filled circles labeled 1960, 1880, and 1785 represent calculated points at three temperatures and fixed composition which illustrate the calculated temperature dependence.
3. Activities of FeO in iron saturated CaO-FeO-SiO₂ at 1550°C. Dashed lines are from Timucin and Morris²⁰ and the solid lines represent our calculations.

REFERENCES

1. P. L. Lin and A. D. Pelton, *Metall. Trans.* **10B**, 667-676 (R1979).
2. C. R. Masson, I. B. Smith, and S. G. Whiteway, *Can. J. Chem.* **48**, 1456-1464 (1977); *Proc. 11th International Congress on Glass*, J. Gotz, Ed., Vol. 1, pp. 3-41, Prague (1977).
3. D. R. Gaskell, *Metall. Trans.* **8B**, 131-145 (1977).
4. C. J. B. Fincham and F. D. Richardson, *Proc. Roy. Soc.* **223**, 40 (1954).
5. G. W. Toop and C. S. Samis, *Trans. TMS-AIME* **224**, 878-887 (1962).
6. M. Blander, "Thermodynamic Properties of Molten Salt Solutions," *Molten Salt Chemistry*, M. Blander, Ed., Interscience, N.Y., pp. 127-237 (1964).
7. M. Blander and A. D. Pelton, Computer Assisted Analyses of the Thermodynamic Properties of Slags in Coal Combustion Systems, ANL/FE-83-19, Argonne National Laboratory, Argonne, IL (1983) Available from NTIS, U.S. Dept. of Commerce, Washington, D.C.
8. M.-L. Saboungi and M. Blander, *J. Chem. Phys.*, **63**, 212-220 (1975); *J. Amer. Ceram. Soc.* **58**, 1-7 (1975).
9. A. D. Pelton and M. Blander, in preparation.
10. A. Muan and E. F. Osborne, Phase Equilibria Among Oxides in Steelmaking, Addison-Wesley Publishing Co., Reading, Mass. (1965).
11. R. A. Sharma and F. D. Richardson, *J. Iron Steel Inst.* **200**, 373 (1962); **198**, 308 (1961).
12. R. H. Rein and J. Chipman, *Trans. AIME* **233**, 415-425 (1965).
13. R. A. Robie, B. S. Hemingway, and J. R. Fisher, Thermodynamic Properties of Minerals and Related Substances at 298.15 K and 1 Bar Pressure and at Higher Temperatures, Geologic Survey Bulletin 1452, U.S. Govt. Printing Office, Washington, D.C. (1978).
14. Ya. I. Ol'shanskii, *Dokl. Akad. Nauk. SSR* **76**, 94 (1951); J. D. Tewhey and P. C. Hess, *Phys. Chem. Glasses*, **20**, 41-53 (1979).
15. J. F. Elliott, *Trans. AIME*, **203**, 485 (1955).
16. P. A. Distin, S. G. Whiteway, and C. R. Masson, *Can. Met. Quart.*, **10**, 73(1971).
17. R. Schuhmann and P. Ensio, *J. Metals*, **3**, 401 (1951).
18. C. Bodsworth, *J. Iron and Steel Inst., London*, **193**, 13 (1959).
19. E. M. Levin, C. R. Robbins, and H. F. McMurdie, Phase Diagrams for Ceramists, Am. Ceram. Soc., Columbus, Ohio (1964); Supplement, (1969); E. M. Levin and H. F. McMurdie, Supplement (1975).
20. M. Timucin and A. E. Morris, *Met. Trans.*, **1**, 19 (1970).
21. M. Blander, "Some Fundamental Concepts in the Chemistry of Molten Salts" in Molten Salts, G. Mamantov, ed., Marcel Dekker, New York (1969).
22. H. Gaye and P. Riboud, Données Experimentales sur les Activités des Constituants de Laitiers, IRSID PCM-RE 337, St. Germain-en-Laye, France (1976).

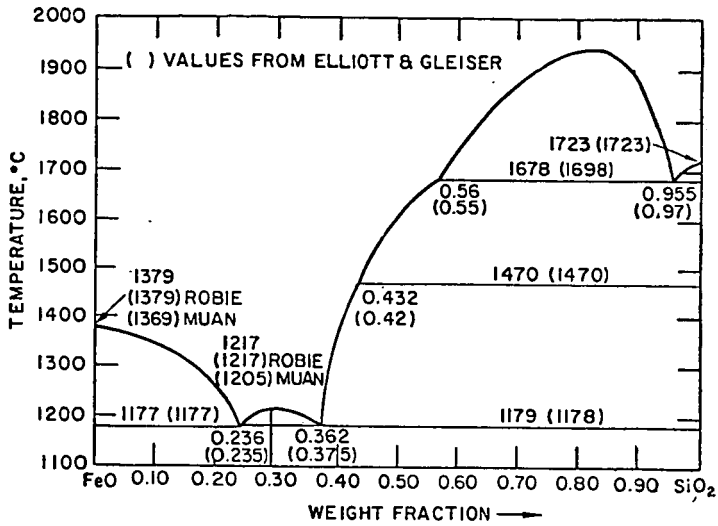


Fig. 1

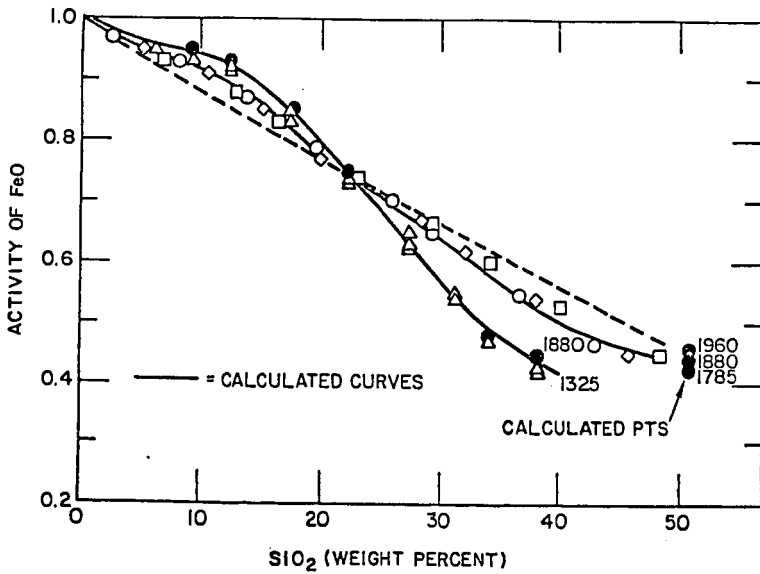


Fig. 2

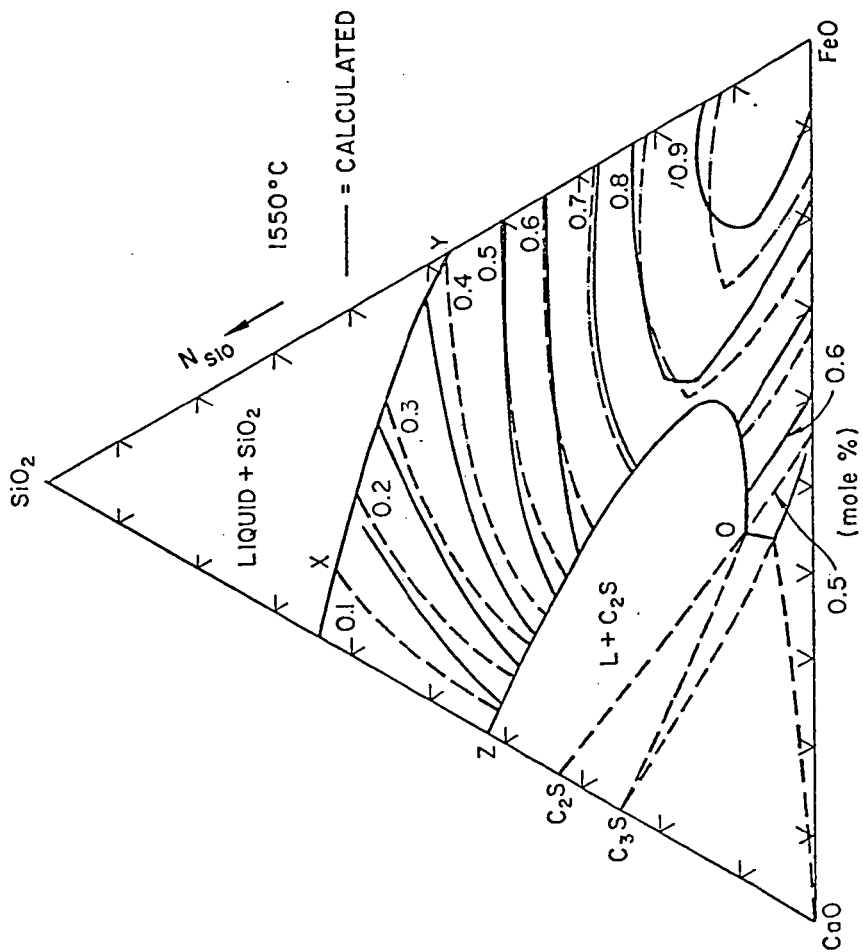


FIG. 3